Calhoun: The NPS Institutional Archive

DSpace Repository

Theses and Dissertations | 1. Thesis and Dissertation Collection, all items

1987

Measurement of particle size distribution in a solid propellant rocket motor using light scattering.

Pruitt, Ted E.

http://hdl.handle.net/10945/22832

Downloaded from NPS Archive: Calhoun

http://www.nps.edu/library

Calhoun is the Naval Postgraduate School's public access digital repository for research materials and institutional publications created by the NPS community. Calhoun is named for Professor of Mathematics Guy K. Calhoun, NPS's first appointed -- and published -- scholarly author.

Dudley Knox Library / Naval Postgraduate School
411 Dyer Road / 1 University Circle
Monterey, California USA 93943

DUDLEY KNOX LIBRARY
NAVAL POSTGRADUATE SCHOOL
MONTEREY, CALIFORNIA 93943-5002

NAVAL POSTGRADUATE SCHOOL
Monterey, California

THESIS

MEASUREMENT OF PARTICLE SIZE DISTRIBUTION IN A SOLID PROPELLANT ROCKET MOTOR USING LIGHT SCATTERING

by

Ted E. Pruitt

June 1987

Thesis Advisor: D. W. Netzer

Approved for public release; Distribution is unlimited

T233638

SECURITY CLASSIFICATION OF THIS PAGE

REPORT DOCUMENTATION PAGE

1a REPORT SECURITY CLASSIFICATION: Unclassified	1b RESTRICTIVE MARKINGS
2a SECURITY CLASSIFICATION AUTHORITY	3 DISTRIBUTION/AVAILABILITY OF REPORT: Approved for public release; distribution is unlimited
2b DECLASSIFICATION/DOWNGRADING SCHEDULE	
4 PERFORMING ORGANIZATION REPORT NUMBER(S)	5 MONITORING ORGANIZATION REPORT NUMBER(S)
6a NAME OF PERFORMING ORGANIZATION: Naval Postgraduate School; 6b OFFICE SYMBOL (If applicable): 67	7a NAME OF MONITORING ORGANIZATION: Naval Postgraduate School
6c ADDRESS (City, State, and ZIP Code): Monterey, California 93943-5000	7b ADDRESS (City, State, and ZIP Code): Monterey, California 93943-5000
8a NAME OF FUNDING/SPONSORING ORGANIZATION: Air Force Rocket Propulsion Laboratory; 8b OFFICE SYMBOL (If applicable)	9 PROCUREMENT INSTRUMENT IDENTIFICATION NUMBER
8c ADDRESS (City, State, and ZIP Code): Edwards AirForce Base, California 93523	10 SOURCE OF FUNDING NUMBERS: PROGRAM ELEMENT NO; PROJECT NO F04611-86-X-0008; TASK NO; WORK UNIT ACCESSION NO

11 TITLE (Include Security Classification)
MEASUREMENT OF PARTICLE SIZE DISTRIBUTION IN A SOLID PROPELLANT ROCKET MOTOR USING LIGHT SCATTERING

12 PERSONAL AUTHOR(S)
Ted E. Pruitt

13a TYPE OF REPORT	13b TIME COVERED	14 DATE OF REPORT (Year Month Day)	15 PAGE COUNT
Master's Thesis	FROM _____ TO _____	1987 June	94

16 SUPPLEMENTARY NOTATION

17 COSATI CODES			18 SUBJECT TERMS (Continue on reverse if necessary and identify by block number)
FIELD	GROUP	SUB-GROUP	Solid propellant; rocket motor; light scattering; particle size distribution

19 ABSTRACT (Continue on reverse if necessary and identify by block number)

Research was conducted to determine the particle size distribution in the motor and exhaust of a small solid propellant rocket motor using light scattering techniques. A commercially produced MALVERN 2600 Particle Sizer was used in conjunction with a locally designed light scattering apparatus. The physical dimensions of the motor windows limited the minimum measurable particle size to roughly 3.5 microns. Motor data was repeatable and agreement between light scattering systems was within approximately 7%. A large particle bias was evident. The source of this bias was believed to be the RTV used for bonding and inhibiting. Design of a new slender two-dimensional

20 DISTRIBUTION/AVAILABILITY OF ABSTRACT	21 ABSTRACT SECURITY CLASSIFICATION
☒ UNCLASSIFIED/UNLIMITED ☐ SAME AS RPT ☐ DTIC USERS	Unclassified
22a NAME OF RESPONSIBLE INDIVIDUAL: D. W. Netzer	22b TELEPHONE (Include Area Code): (408) 646-2980; 22c OFFICE SYMBOL: Code 67 Nt

DD FORM 1473, 84 MAR — 83 APR edition may be used until exhausted. All other editions are obsolete.

SECURITY CLASSIFICATION OF THIS PAGE

#19 - ABSTRACT - (CONTINUED)

motor was completed to permit smaller particle sizes to be measured within the combustor.

Approved for public release; distribution is unlimited.

Measurement of Particle Size Distribution in a Solid Propellent Rocket Motor Using Light Scattering

by

Ted E. Pruitt
Lieutenant Commander, United States Navy
B. E., Vanderbilt University, 1977

Submitted in partial fulfillment of the
requirements for the degree of

MASTER OF SCIENCE IN ENGINEERING SCIENCE

from the

ABSTRACT

Research was conducted to determine the particle size distribution in the motor and exhaust of a small solid propellant rocket motor using light scattering techniques. A commercially produced MALVERN 2600 Particle Sizer was used in conjunction with a locally designed light scattering apparatus. The physical dimensions of the motor windows limited the minimum measurable particle size to roughly 3.5 microns. Motor data was repeatable and agreement between light scattering systems was within approximately 7%. A large particle bias was evident. The source of this bias was believed to be the RTV used for bonding and inhibiting. Design of a new slender two-dimensional motor was completed to permit smaller particle sizes to be measured within the combustor.

TABLE OF CONTENTS

I. INTRODUCTION.....11

II. THEORETICAL BACKGROUND.....14

III. EXPERIMENTAL APPARATUS.....18

A. INTRODUCTION.....18

B. ROCKET MOTOR.....18

C. LIGHT SCATTERING APPARATUS.....22

D. DATA ACQUISTION AND REDUCTION.....26

IV. RESULTS AND DISCUSSION.....28

A. INTRODUCTION.....28

B. TWO-DIMENSIONAL ROCKET MOTOR DESIGN.....28

C. SYSTEM CALIBRATION.....36

D. BEAM WANDER.....42

E. MOTOR FIRINGS.....45

V. CONCLUSIONS AND RECOMMENDATIONS.....89

LIST OF REFERENCES.....91

INITIAL DISTRIBUTION LIST.....93

LIST OF TABLES

I. LASER SPECIFICATIONS.....21

II. 2D CONVERGING NOZZLE DIMENSIONS.....35

III. SUMMARY OF MOTOR FIRINGS.....48

IV. SUMMARY OF EXPERIMENTAL RESULTS.....49

LIST OF FIGURES

3.1 Motor Components.....19

3.2 Motor on Test Stand, Horizontal Mounting.....20

3.3 NPS Light Scattering Apparatus.....23

3.4 MALVERN Particle Sizing System.....25

4.1 Sketch of Proposed 2D Motor.....29

4.2 Comparative Test Profile, NPS System.....38

4.3 Initial Comparative Test Results, MALVERN Using All 31 Diode Rings.....39

4.4 Final Comparative Test Results, MALVERN Using Inner 28 Diode Rings.....41

4.5 Calibration Profile for 9.6 Micron Spheres in Motor Cavity, NPS System.....43

4.6 Low Voltage Exhaust Profile.....51

4.7 Volume Distribution Motor Results Using Inner 28 Diode Rings, 5 May.....52

4.8 Volume Distribution Motor Results Using Inner 28 Diode Rings, 6 May.....53

4.9 Number Distribution Motor Results Using Inner 28 Diode Rings, 5 May.....55

4.10 Number Distribution Motor Results Using Inner 28 Diode Rings, 6May.....56

4.11 Volume Distribution Motor Results Using Inner 28 Diode Rings, 7 May.....57

4.12 Number Distribution Motor Results Using Inner 28 Diode Rings, 7 May.....58

4.13 Propellant Chamber Pressure, 12 May.....60

4.14 Exhaust Profile, 12 May.....61

4.15 Exhaust Profile, 13 May.....62

4.16 Volume Distribution Motor Results Using Inner 28 Diode Rings, 12 May.....64

4.17 Number Distribution Motor Results Using Inner 28 Diode Rings, 12 May.....65

4.18 Volume Distribution Motor Results Using Inner 28 Diode Rings, 13 May.....66

4.19 Number Distribution Motor Results Using Inner 28 Diode Rings, 13 May.....67

4.20 SEM Photograph of Collected Combustion Products Near Windows, 1.0% ZrC.....68

4.21 SEM Photograph of Collected Combustion Products In Graphite Nozzle, 1.0% ZrC.....68

4.22 SEM Photograph of Collected Combustion Products In Graphite Nozzle, 1.0% ZrC.....69

4.23 High Speed VCR Prints of Partial Nozzle Blockage....71

4.24 Exhaust Profile, 19 May.....74

4.25 Exhaust Profile, 20 May.....75

4.26 Volume Distribution Motor Results Using Inner 28 Diode Rings, 19 May.....76

4.27 Number Distribution Motor Results Using Inner 28 Diode Rings, 19 May.....77

4.28 Volume Distribution Motor Results Using Inner 28 Diode Rings, 20 May.....78

4.29 Number Distribution Motor Results Using Inner 28 Diode Rings, 20 May.....79

4.30 SEM Photograph of Collected Combustion Products in Graphite Nozzle, 2.0% Al.....80

4.31 SEM Photograph of Collected Combustion Products in Graphite Nozzle, 2.0% Al.....80

4.32 SEM Photograph of Collected Combustion Products in Graphite Nozzle, 2.0% Al.....81

4.33 Volume Distribution Exhaust Results, 22 May.....83

4.34 Number Distribution Exhaust Results, 22 May.....84

4.35 Volume Distribution Exhaust Results, 26 May.....85

4.36 Number Distribution Exhaust Results, 26 May.....86

4.37 Motor Profile, 22 May.....87

4.38 Motor Profile, 26 May.....88

ACKNOWLEDGEMENTS

I would like to acknowledge the guidance and assistance of Professor David W. Netzer whose positive attitude and leadership provided the foundation for successful completion of this investigation. The technical support of Mr. Harry Conners, Mr. Pat Hickey, and Mr. Don Harvey was greatly appreciated.

I. INTRODUCTION

Aluminum is used as a solid propellant additive to improve rocket performance. A burning propellant containing aluminum delivers a higher specific impulse and more effectively dampens high frequency acoustic oscillations. These gains in motor performance are counter-balanced by a lowered specific impulse efficiency resulting from two-phase flow loses in the nozzle, incomplete aluminum particle combustion, and nozzle erosion. The major contributors to reduced efficiency by two-phase flow losses are particle-gas velocity lags and the fact that the particles do not "expand" as they pass through the nozzle..

The burning aluminum often produces a bi-modal distribution of aluminum oxide particle sizes. Aluminum particles that leave the burning propellant surface shortly after exposure and burn in the gas stream produce oxide particles of less than 1-2 microns in diameter. These smaller particles contribute to exhaust plume signature. They also contribute to two-phase flow losses, but little can be done to further decrease the losses. Particles that do not leave the propellant surface immediately may agglomerate as they melt and burn, and the oxide layer they produce can break free from the surface in sizes larger than 5 microns [Ref. 1]. These larger particles are a major

contributor to the two-phase flow loss, and their effect can be minimized by reducing their size.

There are several complex, semi-empirical, computer programs that attempt to model the most important momentum and thermal energy exchange processes, and predict particle sizes in the exhaust nozzle. These models are based on collected samples from small rocket motor exhausts [Ref. 2] and have not been validated for accuracy in particle size predictions inside the rocket motor and exhaust nozzle. Non-intrusive measurements of particles between the propellant surface and the rocket exhaust using laser holography and high speed photography have produced some substantiated data for particles larger than approximately 18 microns [Ref. 1]. These methods have not proven successful for smaller particles which represent the majority of those present.

Two additional non-intrusive methods for conducting measurements are light transmission and light scattering, each having advantages and disadvantages. Light scattering techniques are generally considered to be applicable only in environments where the transmittance is greater than 90% in order to satisfy single scattering requirements assumed by the data analysis programs. Light transmission techniques which are applicable to dense concentrations, including multiple scattering environments, work best for small particles, roughly the wavelength of the illumination source, and require a-priori knowledge of particle

characteristics [Ref. 1]. At present, light scattering is the most promising technique for extending the data base to particles in the size range of 0.5-18 microns, without detailed knowledge of particle characteristics. It also has the advantage of extending up into the particle sizes measurable by holography and high speed photography, which will provide additional verification of data obtained by those techniques.

To date, the investigative goal has been to develop verifiable, experimental techniques for obtaining quantitative light scattering data. Once the techniques are developed, they will be used to determine the effects of propellant properties, operating pressures, and nozzle geometries on the behavior of particulates at various positions within the rocket motor and exhaust nozzle. These results are needed to provide data on the effect of metal and metal oxide size distributions on rocket motor performance, flow losses, and exhaust signature. They are also needed as feedback to improve the accuracy of the computer models presently used in predicting the rocket motor internal operating environment and exhaust plume signature. A summary of previous investigations conducted at the Naval Postgraduate School facilities and the associated results can be obtained from Reference 1.

II. THEORETICAL BACKGROUND

The method used in the present investigation was the diffractively scattered light technique. This method measures the diffraction patterns of light scattered by particles and analyzes the data obtained to determine mean diameters, such as the volume-to-surface mean diameter (D_{32}), and distributions of particle sizes. The non-intrusive nature of data collection, by measuring the diffraction patterns of scattered light, makes this a preferable technique for the internal rocket motor environment. The major disadvantages of this technique are (1) the difficulty in determining size distributions, (2) bias in the determined values attributable to the limitations imposed by maximum and minimum angles of measurable scattered light, (3) maximum limits on the total concentrations of particulates allowed to limit multiple scattering and (4) the difficulty of keeping viewing windows free from particle deposition.

The general theory of light scattering was developed by Mie. His equations were not limited to any particular particle size or refractive index. These complex equations containing Legendre polynomials and spherical Bessel functions are applicable to all situations, but are very

cumbersome for data reduction. Van de Hulst [Ref. 3] provides a detailed discussion of the light scattering characteristics of spherical particles, including considerations for reflection, refraction, diffraction and absorption.

When the particle size is significantly different from the wavelength of the scattered light, the less complicated theories of Rayleigh (size much less than the wavelength of scattered light) or Fraunhofer (size much greater than the wavelength of scattered light) may be used. Fraunhofer diffraction has been successfully applied to particles with diameters of approximately the wavelength of the illumination source. The wavelength of the light sources used in this investigation was 632.8 nm, provided by two different He-Ne laser systems. The maximum measurable scattering angles of the locally designed system and the commercially produced MALVERN 2600 series system fixed the minimum detectable particle size to approximately 3.0 microns and 0.5 microns, respectively. These physical limitations restricted the area of interest to Fraunhofer diffraction.

Both theory and data collected to date suggest that the particle sizes found in solid propellant rocket motors are polydispersed and often bi-modal. Particle size determination, or more correctly particle size distribution determination, for a polydispersion is difficult because the

discrete ring patterns for the scattered light from individual particles do not exist. However, Dobbins, et al [Ref. 4] found that for a polydispersion D_{32} can be accurately measured. D_{32} is defined by

$$D_{32} = \int_0^{D_{max}} N_r(D) D^3 dD \Big/ \int_0^{D_{max}} N_r(D) D^2 dD \ ,$$

where $N_r(D)$ is a distribution function describing the proportion of particles with diameter D in the sample. Dobbins, et al [Ref. 4] used the Upper-Limit-Distribution-Function (ULDF) developed by Mugele and Evans [Ref. 5], and this approach was followed in the locally designed laser system used in this investigation. The Introduction chapters of References 6-9 provide a complete overview of the implemented theory for the locally designed system.

Reference 4 shows D_{32} to be quite insensitive to the form of $N_r(D)$. This fact allowed D_{32} to be the common aspect for comparison of results between the MALVERN 2600 series Particle Sizer (ring diode arrays) and the previously used and locally designed, linear diode array system. This allowed the MALVERN's ability to measure particle distributions to be employed in a somewhat verifiable manner, even though the data reduction algorithm for the

MALVERN Particle Sizer is proprietary and, therefore, not available to the user.

The reference manual for the MALVERN [Ref. 10] (Page 1-1) states that the "Model Independent" mode, a non-linear least squares analysis method, is able to measure multimodal particle sizes with high resolution. Finally, during a phone conversation with Mr. John Taylor of Malvern Instruments, Inc. he indicated that the "Model Independent" mode is based entirely on Fraunhofer diffraction.

III. EXPERIMENTAL APPARATUS

A. INTRODUCTION

Photographs of the rocket motor are presented in Figures 3.1 and 3.2. They respectively show the disassembled motor and the assembled motor horizontally mounted. The following major modifications were made to the motor and measurement apparatus used in the previous investigation:

- The motor mounting brackets were modified and the motor was horizontally mounted,
- One of the two locally designed He-Ne laser systems was replaced by the MALVERN 2600 Series Particle Sizer, and,
- The Hewlett Packard 9836S data acquistion program was modified to provide the necessary switching to externally trigger the MALVERN 2600.

Table I gives the specifications for the lasers used.

B. ROCKET MOTOR

The motor used in this investigation differed in three minor aspects to that used by Keith [Ref. 9]. First, graphite nozzles were used, extending the motor length by one inch. Secondly, most motor firings were conducted using a cylindrical 2" diameter by 1" to 1.25" thick, non-perforated (end burning) propellant. And, near the end of the investigation, a 4" extension was added to the port

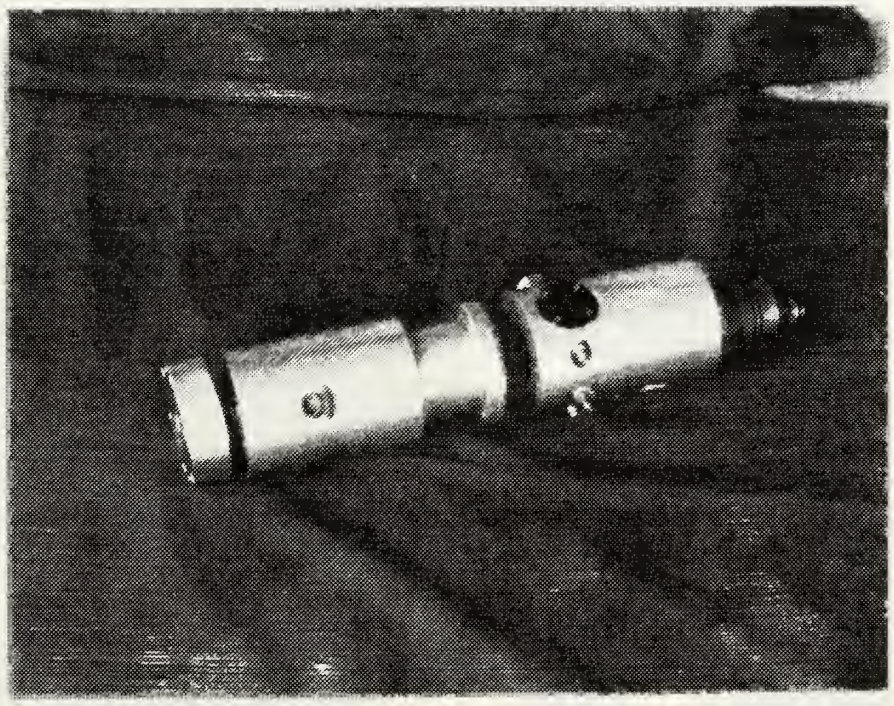

Figure 3.1 Motor Components

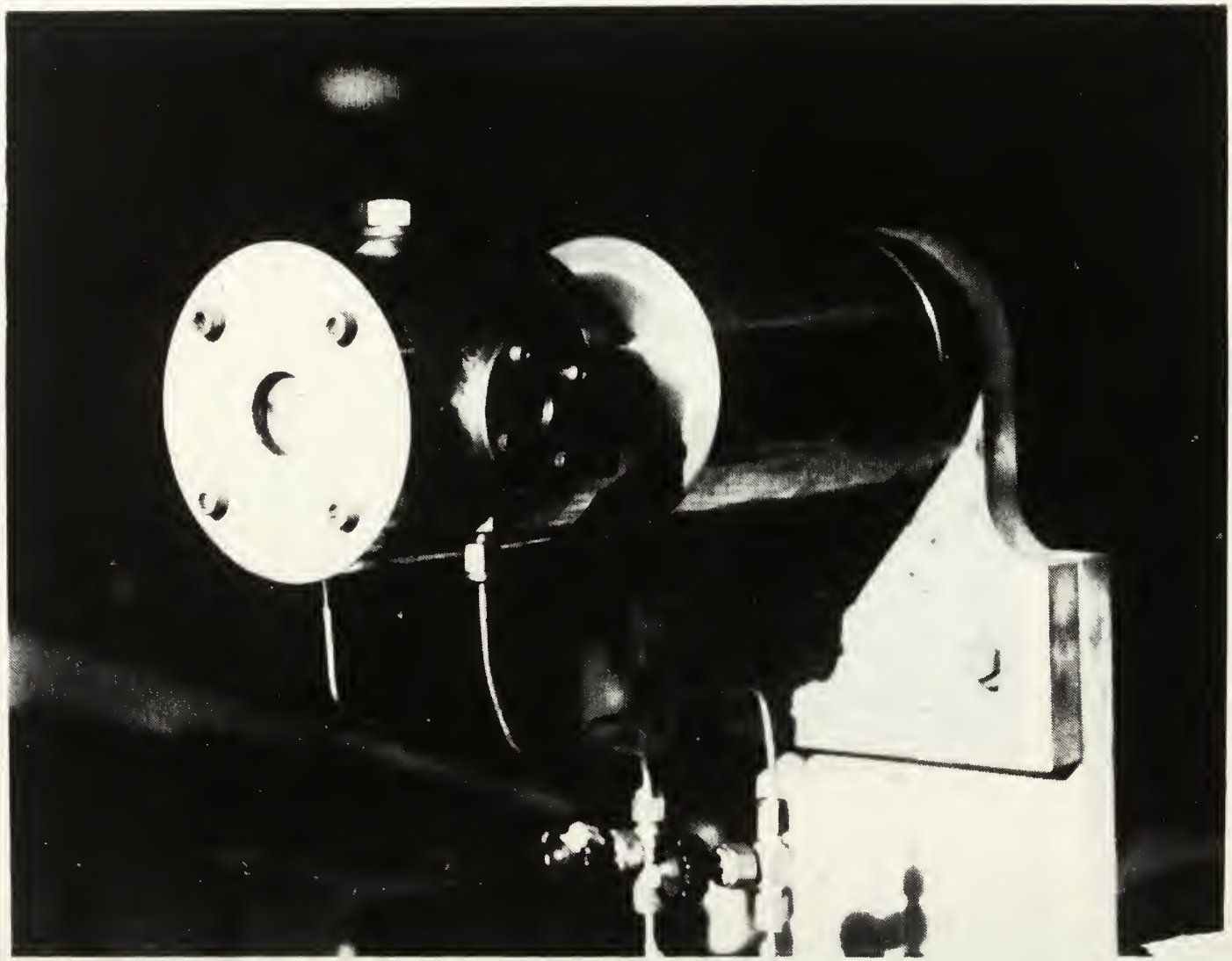

Figure 3.2 Motor on Test Stand, Horizontal Mounting

TABLE I

LASER SPECIFICATIONS

A. Helium-Neon Laser (Locally Designed System)

1.	Manufacturer:	Spectra-Physics
2.	Model:	147
3.	Type:	He-Ne Class IIIB
4.	Output Power:	8 mWatt
5.	Beam Diameter:	.92mm
6.	Beam Divergence:	.87 mrad

B. Helium-Neon Laser (Commercial System)

1.	Manufacturer:	MALVERN Instruments
2.	Model:	2600
3.	Type:	He-Ne Class IIIB
4.	Output Power:	2 mWatt
5.	Beam Diameter:	9 mm
6.	Beam Divergence:	Not Available

containing the rupture disc to prevent disc failure from direct exposure to burning metals.

Two quite different composite propellants were used in the motor firings. The first contained 1%, by weight, of 6 micron zirconium-carbide (ZrC) which was not expected to burn at the nominal combustion gas temperature. The second, contained 2%, by weight, of 40 micron aluminum. The aluminum should completely oxidize at nominal gas temperatures, with a 10-15 msec residence time. Both propellants were ignited using a $BKNO_3$ igniter fired by heating a high resistance nichrome filament with a 12 VDC source.

C. LIGHT SCATTERING APPARATUS

The light scattering apparatus previously used by Keith [Ref. 4] is shown in the photograph of Figure 3.3, positioned to measure in the motor exhaust. Page 6 of Reference 1 provides a complete description of this apparatus.

The new light scattering system introduced by this investigation was the MALVERN 2600 Series Particle Sizer. This is a commercial system, manufactured and distributed by MALVERN Instruments of Malvern, England. The details of the sizing theory and analysis programs are considered to be

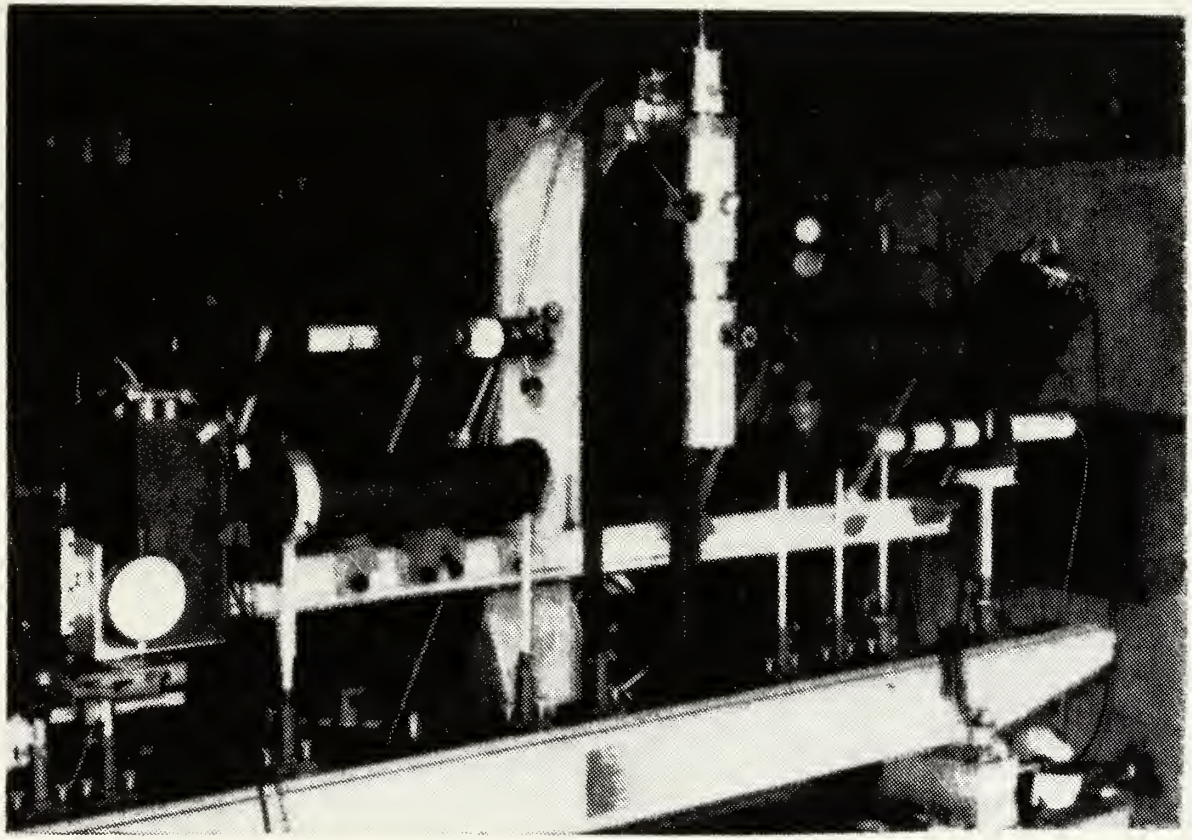

Figure 3.3 NPS Light Scattering Apparatus

proprietary in nature by the manufacture and could not be obtained.

The MALVERN 2600, depicted in Figure 3.4, uses a 2 mW, He-Ne Laser (632.8 nm wavelength) with a 9 mm diameter, collimated, and spatially filtered beam [Ref. 11]. The illumination source and detector are mounted on a rigid optical bench. The detector uses three interchangable Fourier Transform Lens with focal lengths of 63, 100, and 300 mm [Ref. 11]. Their respective particle sizing ranges are 1.2-118, 1.9-188, and 5.8-564 microns, with a sub-class down to 0.5 microns [Ref. 10]. When the sub-class is included, the dynamic range is 180:1 on any of the three range settings with an advertized accuracy of +/- 4% on Volume Median Diameter [Ref. 11]. The 100 mm lens with a particle range of 1.9-188 microns was used during this investigation.

The MALVERN 2600 detector uses a 31 element solid state array of concentric semicircular diode rings. The 31 rings are sampled in parallel through individual amplifiers. The sample/hold electronic construction uses A/D conversion and on board digital storage. This electronic arrangement provides a sampling time of 10-15 microseconds, overcoming the limitation imposed by a minimum computer read in time of approximately 25 msec.

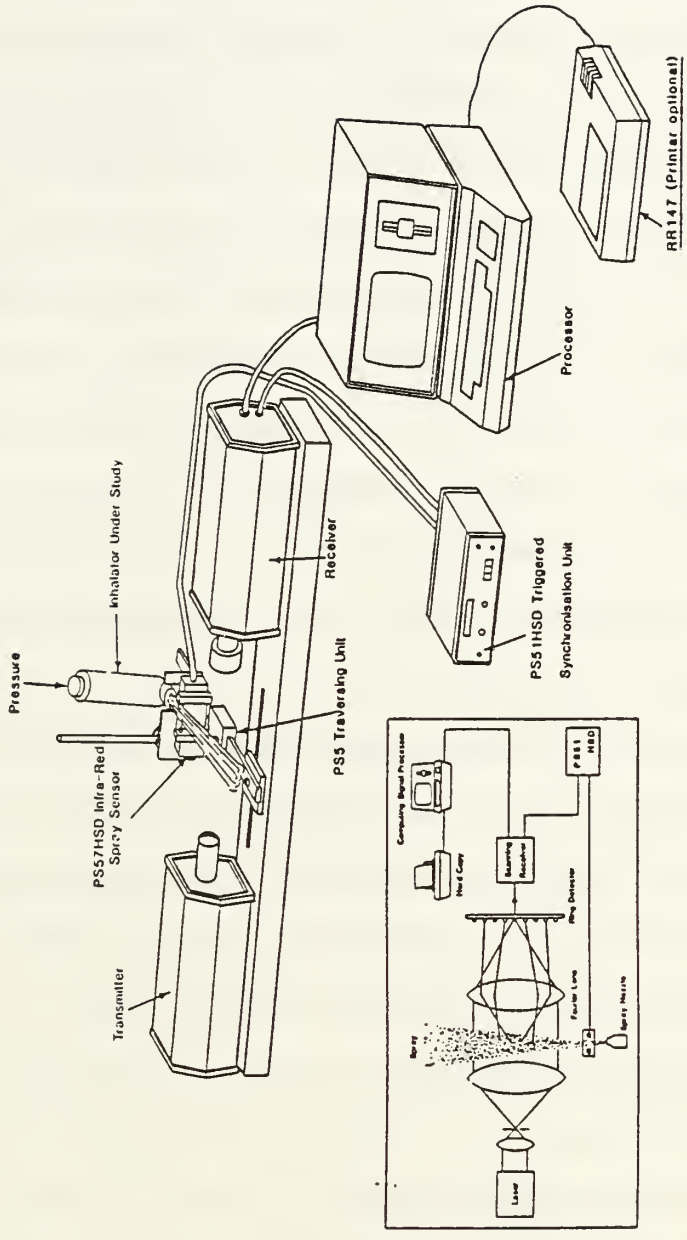

Figure 3.4 MALVERN Particle Sizing System (Ref. 11)

D. DATA ACQUISITION AND REDUCTION

Data from the locally designed system was acquired in accordance with the computer program developed by Harris [Ref. 12]. The detector's own circuit board provided a sample and hold, amplified signal. The data was scanned at 33 KHz and then stored in a Hewlett Packard HP6942A multiprogramer. System control was accomplished using a HP9836S computer. Manual triggering was used in the early motor firings of this investigation, using operator interface via the HP9836S keyboard. Preprogrammed automatic triggering at 150 psi plus a 1.2 second time delay, was used for the final four runs.

The computer program developed by Harris and modified by Rosa [Ref. 7] was used for data reduction, with the modification that the background light noise was not subtracted from the measured data during the testing period of 19-26 May. This was accomplished by deleting the subtraction of the background data matrix on line 1470 of the "RDC1" program. Four scans of the linear diode array were used in both the exhaust and motor configurations. The low-level background was not subtracted because of a problem with several of the diodes on the 1024 element array.

The MALVERN 2600 Particle Sizer also provides A/D conversion, plus local storage in the diode array circuitry. System control in the manual mode (internal trigger) was

provided by operator interface, via the keyboard of the MALVERN system's AT&T 6300PC. The automatic mode (external trigger) was controlled by the HP9836S simultaneously with the locally designed system. This was incorporated by using a 100 Hz signal generator to provide a 5.0 volt, triangular wave to trigger the MALVERN'S Spray Synchronizer, which provides triggering control to the MALVERN in the external mode. This external trigger signal was supplied via a switching network in the HP9836S computer system. Harris' computer program [Ref. 12] was modified to close the switch at the sample initiation point in the program and to open the switch after a 3 second time delay.

Data acquisition was accomplished using the MALVERN's MASTER-SIZER operating system. This operating system uses a command based language that allows the user to specify the instrument operations and analysis restrictions. Section 4.1 of Reference 11 provides a complete description of the MASTER-SIZER operating system. The "Model Independent" analysis program is able to measure multimodal particle sizes [Ref. 10], and was used exclusively for reduction of MALVERN data. This program uses non-linear least squares analysis to find the size distribution which most closely fits the measured scattering profile [Ref. 10]. The remaining three models, Rosin-Rammler, Log-Normal and Normal functions, are monomodal analysis programs and were not felt to be appropriate for the present investigations.

IV. RESULTS AND DISCUSSION

A. INTRODUCTION

This investigation was based on four major objectives: (1) design a new two-dimensional motor to optimize use of the MALVERN 2600 Particle Sizer and the locally designed system, (2) incorporate the MALVERN 2600 Particle Sizer into the present three-dimensional motor data collection system, (3) correct the beam wander problem encountered by Keith [Ref. 9] when using the locally designed (NPS) system for motor measurements, and (4) conduct motor firing tests of a repeatable nature to provide cross validation of the two light scattering apparatuses. The goal of previous NPS investigations using light scattering techniques was to determine the D_{32} of the particles in the motor and the nozzle exhaust. With the inclusion of the MALVERN 2600 this investigation would also be able to provide information concerning the particle size distribution in the motor and nozzle exhaust. D_{32} was to be the common analysis parameter used for cross validation.

B. TWO-DIMENSIONAL ROCKET MOTOR DESIGN

A new two-dimensional, slender-ported motor design, Figure 4.1, was desired to optimize the use of both the

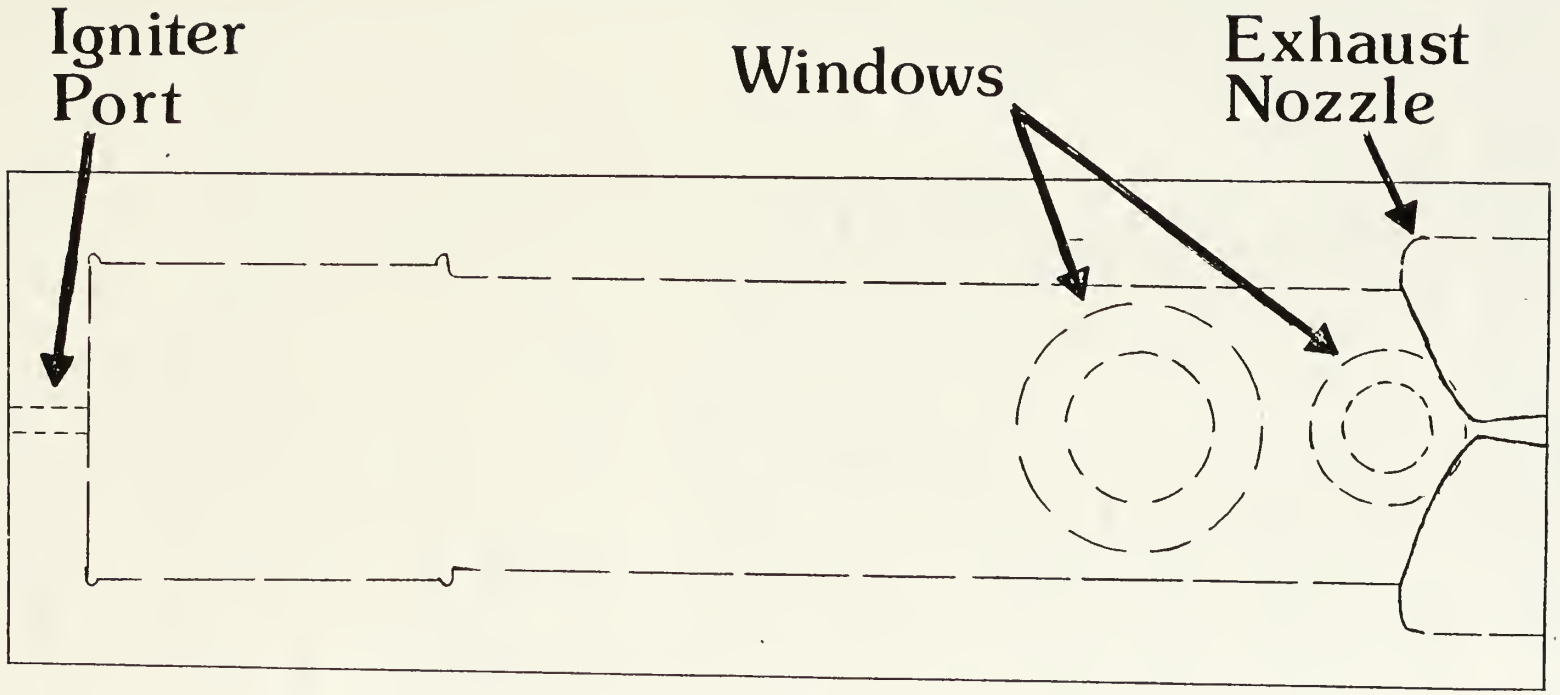

Figure 4.1 Sketch of Proposed 2D Motor

MALVERN and the locally designed system, and to minimize adverse effects on light scattering and holography by reducing the transmission path length through the rocket motor. The motor was to operate at 500, 300, or 100 psia using slabs of solid propellant. The converging nozzle contour was to provide an equivelant rate of change of area to that of a 3-D nozzle with a 30° converging section. This would continue the accumulation of particle break-up and particle-nozzle interaction data which could be directly related to the previously gathered 3-D data, while taking advantage of the narrow transmission path length of the 2-D design. Generic constants that approximated the propellants in use were used to aid in verification of the feasibility of design. These constants were:

$a=0.0304$
$g_c=32.174$ lbm-ft/lbf-sec
$n=0.45$
$C^*=5000$ ft/sec
$\rho=0.062$ lbm/in^3
$T_c=5800$ °R
$R=50$ ft-lbf/lbm-°R
gamma=1.2

To obtain the desired operating pressures, propellant burning surface to nozzle throat area ratios were established using the relationship:

$$P_c = [(A_b a \rho C^*)/(A_{th} g_c)]^{[1/(1-n)]} .$$

Thus for P_c=500 psia, A_b/A_{th}=104.16 and
for P_c=300 psia, A_b/A_{th}= 78.65 and
for P_c=100 psia, A_b/A_{th}= 42.98.

A maximum propellant slab length of 7" was chosen. This maximum length ensured that most solid propellants readily available to NPS, regardless of packaged shape, could be cut to provide one-piece slabs for use in the motor. Choosing a fixed port/propellant width of .25" as the through-motor path length for laser light, and a maximum propellant chamber length of 7", provided a propellant burning surface area of 3.5 in^2 for the two propellant slabs. Combining $A_b(max)$=3.5 in^2 with $P_c(max)$=500 psia and using the above area ratio gives an A_{th} of 0.0336 in^2. With A_{th} now fixed, the propellant slab lengths for chamber pressures of 300 and 100 psia are calculated to be 5.3" and 2.9" respectively, using the area ratios.

The next step in design verification was to determine if the narrow port width of 0.25" would result in choked flow prior to the combustion gases reaching the nozzle (station 2). Using the Energy equation:

$$h_t = C_p T_t = C_p T_2 + (V_2^2/2) \quad \text{, and solving for } T_2$$

gives

$$T_2 = T_t - (V_2^2/2C_p) \quad . \qquad \text{Eqn (1)}$$

Applying the continuity equation to the propellant (assuming r does not vary greatly with length):

$$\dot{m}_2 = \rho_p A_b r \quad , \text{ and with } r = aP^n \text{ , results in}$$

$$\dot{m}_2 = 0.1085 \text{ lbm/sec} \quad \text{for } P_c = 500 \text{ psia.}$$

The continuity equation for the gas is

$$\dot{m}_2 = \rho_2 A_p V_2 = (P_2 A_p V_2 / RT_2) = 0.1085 \text{ lbm/sec} .$$

Solving for V_2:

$$V_2 = 21.7(T_2/P_2) \quad . \qquad \text{Eqn (2)}$$

Next, using the momentum equation:

$$p_1 - p_2 = \rho_2 V_2^2 = (P_2 V_2^2 / RT_2) \text{ , and solving for } p_2$$

$$P_2 = P_1/[1 + (V_2^2/RT_2)] \quad . \qquad \text{Eqn (3)}$$

Substituting Equation (3) into Equation (2) and rearranging:

$$(21.7/R)V_2^2 - P_1 V_2 + 21.7T_2 = 0 . \qquad \text{Eqn (4)}$$

Finally, substituting Equation (1) into Equation (4) and solving using the quadratic equation for the worst case V_2

gives a solution (with p_1 = 500 psia) of

$$V_2 = 907.5 \text{ ft/sec.}$$

This value for V_2 and the fact that C_p = 6R can now be used to solve Equation (1) for

$$T_2 = 4427 \text{ °R} .$$

With T_2 now determined the speed of sound at the propellant exit section can be calculated, resulting in a Mach number of

$$M_2 = V_2/a_2 = 0.31 .$$

Thus, the flow velocity remains in the low subsonic region within the fuel port. Erosive burning effects should be negligible.

It was desired to provide an equivalent rate of change of nozzle area to that of a 30° converging 3-D nozzle with an inlet area of 0.575 in² (representing the 2.3" X 0.25" 2-D nozzle inlet area) and a throat area of 0.0336 in² (representing the 0.1344" X 0.25" 2-D nozzle throat area). The equation for cross sectional area of an axisymmetric, 3-D nozzle

$$A = \pi D^2/4 \qquad \text{Eqn (5)}$$

was used such that

$$D = [D_{in} - 2x\tan 30^\circ], \text{ with } D_{in} = 0.856" . \quad \text{Eqn (6)}$$

Solving the above equation for x

$$x = (1/2\tan 30^\circ)[D_{in} - (4A/\pi)^{1/2}]$$

gives a converging nozzle length of 0.562" for a 3-D nozzle. The 2-D approximation of the 3-D nozzle rate of change of area was then accomplished by inserting values for x in 0.1" increments into Equation (6) to obtain increments of nozzle area with equation (5), and then using the equation for the 2D nozzle

$$h = A/W \quad \text{Eqn (7)}$$

where W is fixed at 0.25". The results are given in Table II.

Prior to determining the diverging nozzle dimensions, the nozzle exit area necessary to provide $P_{exit} = P_{amb}$ for chamber pressures of 500, 300, and 100 psia were calculated. Tables for gamma of 1.2 were used for each of the P_e/P_t or P_e/P_c ratios and the values for A_e/A^* where $A^* = A_{th}$ were read directly from the table. This resulted in exit areas of

TABLE II

2D CONVERGING NOZZLE DIMENSIONS

DISTANCE FROM NOZZLE THROAT X_{th} (inches)	DISTANCE FROM NOZZLE ENTRANCE X_{ent} (inches)	AREA A(X) (inches^2)	HEIGHT OF NOZZLE H (inches)
0.562	0.0	0.575	2.3
0.462	0.1	0.431	1.72
0.362	0.2	0.308	1.23
0.262	0.3	0.205	0.82
0.162	0.4	0.123	0.49
0.062	0.5	0.062	0.25
0.0	0.562	0.0336	0.1344

0.186, 0.124, and 0.060 in^2 respectively. Equation (5) and (7) could then be used with

$$D = [D_o - 2x\tan(\text{theta})] ,$$

where D_o = 0.487, 0.397, 0.277, theta is the angle of divergence, and x represents the distance from each nozzle exit in the direction of the throat.

Nozzle throat erosion as a function of time would result in a decreasing maximum propellant chamber pressure (P_c). A 0.1" flat, constant area throat, was added to the motor design to offset the effects of erosion and extend the operating life of the nozzle inserts.

C. SYSTEM CALIBRATION

A phone conversation with Mr. Chris Hughes of MALVERN Instruments indicated that the MALVERN system would not accurately measure the particle diameters and distributions of polystyrene spheres. Keith [Ref. 9] (page 33) had calibrated the NPS system using a monomodal distribution of 5.1 micron polystryene spheres. The system that both Keith and the current investigation used had provided a $D_{3,2}$ measurement of 5.4 microns. This system was then used as a secondary calibration reference with which to compare the MALVERN 2600.

A metal oxide powder, supplied by MALVERN Instruments, containing particles with a nominal size range of 1-20 microns and a mean diameter of 5-8 microns was suspended in distilled water and used as the comparison medium. A glass container measuring approximately 25 mm wide by 20mm high by 6mm deep was used to hold the comparitive sample, and a glass stirring rod was used to mix the sample during measurements.

At this point of the investigation the apparatuses were arranged so that the NPS system would measure the nozzle exhaust and the MALVERN would measure the internal motor environment. Therefore, when taking measurements using the MALVERN, the sample was placed inside the motor cavity with the nitrogen purge filters and the fused silica windows installed. The standard calibration procedure for the NPS system as described by Harris [Ref. 12] was used for that system. Because of the MALVERN's lower tolerance for light obscuration, the sample used with the NPS system was then diluted by a factor of four prior to its measurement with the MALVERN 2600. The calibration of the MALVERN was conducted in accordance with Reference 11.

The results of this comparative test were at first thought to be fair at best. Figure 4.2 gives the D_{32} obtained from the NPS system, which was 5.5 microns. Figure 4.3 shows the tabulated volume distribution and the associated distribution graph which indicate a D_{32} of 4.5

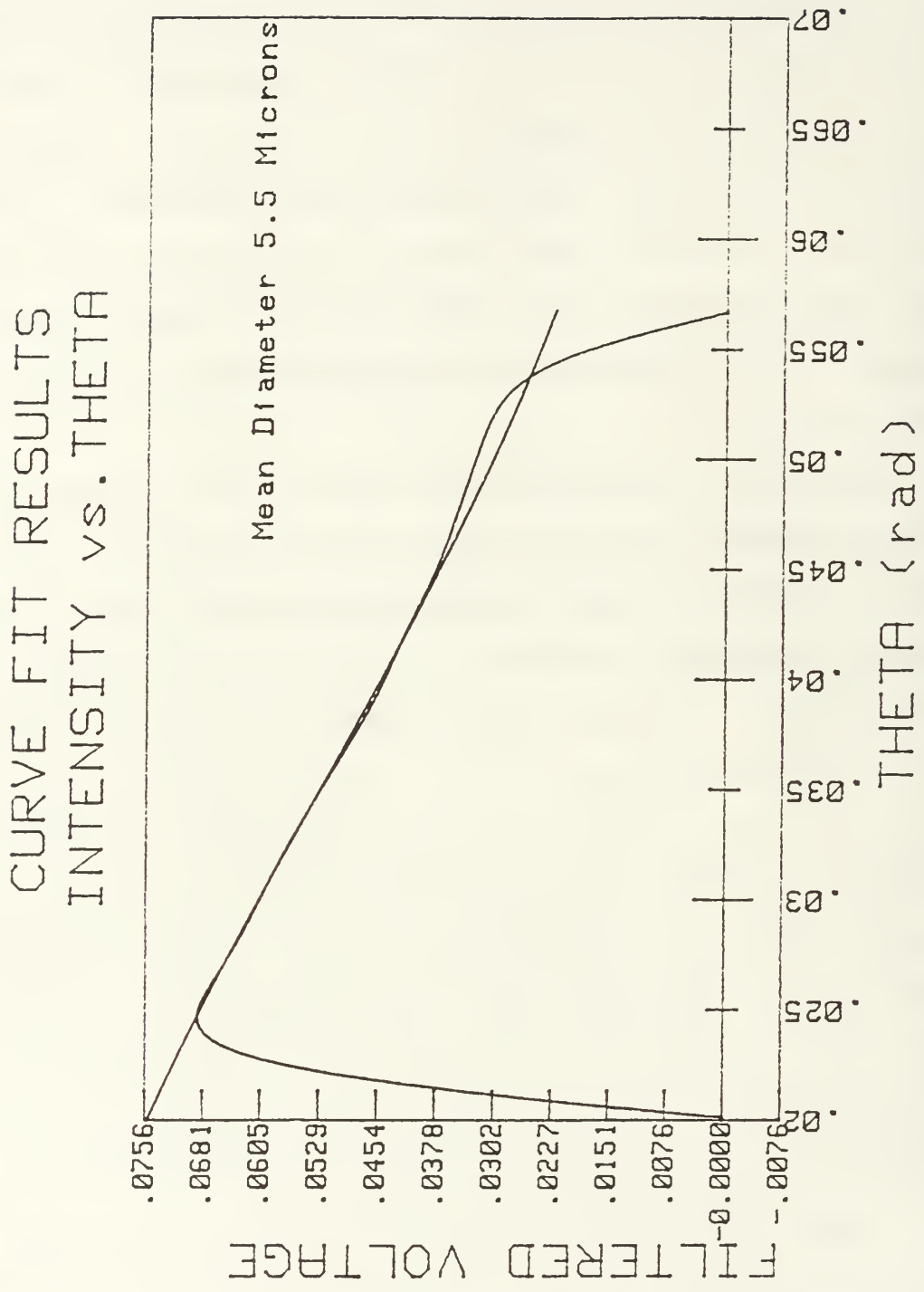

Figure 4.2 Comparative Test Profile, NPS System

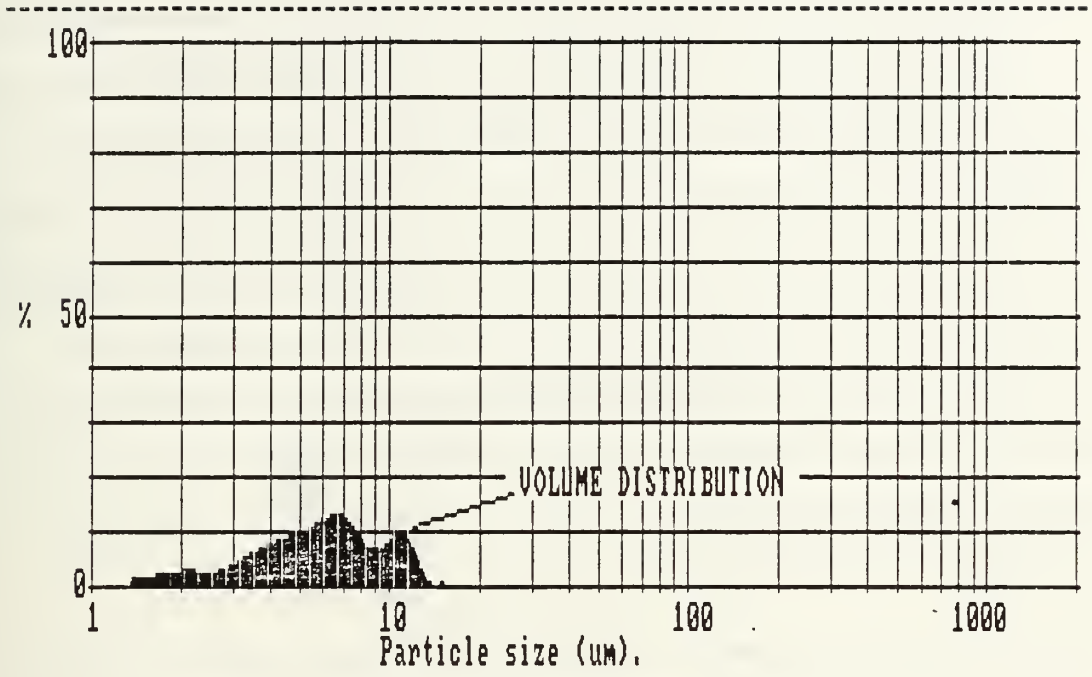

Size microns	under	% in band	Size microns	under	% in band
188.0	100.0	0.0	17.7	100.0	0.2
162.0	100.0	0.0	15.3	99.8	0.3
140.0	100.0	0.0	13.2	99.5	5.4
121.0	100.0	0.0	11.4	94.1	9.7
104.0	100.0	0.0	9.8	84.4	6.5
89.9	100.0	0.0	8.5	77.9	9.2
77.5	100.0	0.0	7.3	68.7	12.6
66.9	100.0	0.0	6.3	56.1	11.7
57.7	100.0	0.0	5.4	44.4	9.6
49.8	100.0	0.0	4.7	34.8	8.2
42.9	100.0	0.0	4.1	26.6	7.0
37.1	100.0	0.0	3.5	19.6	5.1
32.0	100.0	0.0	3.0	14.5	3.0
27.6	100.0	0.0	2.6	11.5	2.5
23.8	100.0	0.0	2.2	9.0	2.7
20.5	100.0	0.0	1.9	6.3	2.5

Result source=testdata
Record No. = 1
Focal length = 100 mm.
Experiment type pil
Volume distribution
Beam length = 6.0 mm.
Obscuration =0.5285
Volume Conc. = 0.0183 %
Log. Diff. =3.17
Model indp

D(v,0.5) = 5.9 µm
D(v,0.9) = 10.7 µm
D(v,0.1) = 2.4 µm
D(4,3) = 6.2 µm
D(3,2) = 4.5 µm
Span = 1.4
Spec. surf. area
0.68 sq.m./cc.

Figure 4.3 Initial Comparative Test Results, MALVERN Using All 31 Diode Rings

microns from the MALVERN. This would indicate that the MALVERN differed from the NPS system by approximately 18%.

Later in the investigation when rocket motor operation had been stabilized and was repeating, the MALVERN data appeared not to repeat. As will be explained in the Motor Firing section, it was discovered that the scattered light received by the outer three rings of the MALVERN was originating from light scattering off the nitrogen purge filter of the window located on the detector side of the motor. This bias could be removed by deleting the data received by the MALVERN's outer three rings using a "KILLDATA 0,3" command in the Master Sizer mode. This limited the MALVERN's measurable particle range to a minimum of 3.5 microns vice the 1.9 microns normally expected when using the 100 mm focal length lens. This would mean that the calculation of D_{32} and the particle distributions would be shifted somewhat, but the fact that a non-linear least squares curve fitting method was used by the Model Independent program meant that for any given particle size distribution the associated curve would most likely remain unique.

After the discovery of the bias being injected by light scattering off the purge filter, the original data, with the outer three rings of data "killed", was reanalyzed. Figure 4.4 shows the tabulated volume distribution and the associated distribution graph which now indicated a D_{32} of

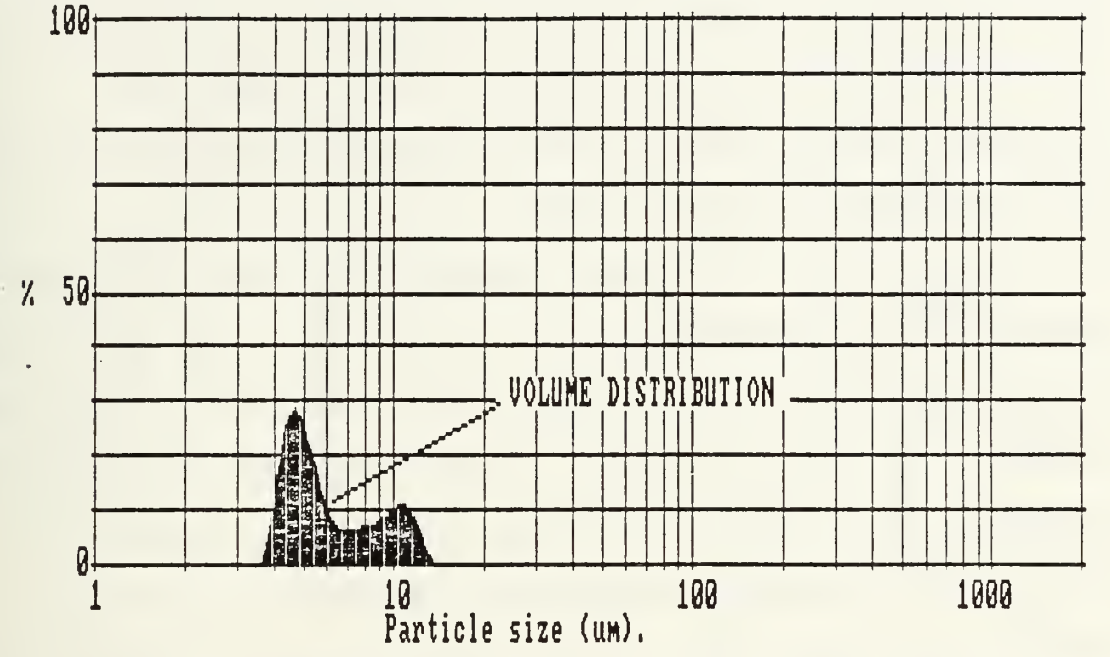

Size microns	under	% in band	Size microns	under	% in band
188.0	100.0	0.0	17.7	100.0	0.0
162.0	100.0	0.0	15.3	100.0	0.0
140.0	100.0	0.0	13.2	100.0	5.4
121.0	100.0	0.0	11.4	94.5	10.9
104.0	100.0	0.0	9.8	83.6	7.9
89.9	100.0	0.0	8.5	75.7	6.4
77.5	100.0	0.0	7.3	69.3	6.2
66.9	100.0	0.0	6.3	63.1	11.7
57.7	100.0	0.0	5.4	51.4	23.9
49.8	100.0	0.0	4.7	27.6	24.6
42.9	100.0	0.0	4.1	3.0	3.0
37.1	100.0	0.0	3.5	0.0	0.0
32.0	100.0	0.0	3.0	0.0	0.0
27.6	100.0	0.0	2.6	0.0	0.0
23.8	100.0	0.0	2.2	0.0	0.0
20.5	100.0	0.0	1.9	0.0	0.0

Result source=testdata
Record No. = 1
Focal length = 100 mm.
Experiment type pil
Volume distribution
Beam length = 6.0 mm.
Obscuration =0.5285
Volume Conc. = 0.0244 %
Log. Diff. =3.15
Model indp

D(v,0.5) = 5.4 µm
D(v,0.9) = 10.7 µm
D(v,0.1) = 4.3 µm
D(4,3) = 6.5 µm
D(3,2) = 5.8 µm
Span = 1.2
Spec. surf. area
0.70 sq.m./cc.

Figure 4.4 Final Comparative Test Results, MALVERN Using Inner 28 Diode Rings

5.8 microns. With the adverse effects of the light scattered by the filter removed, the MALVERN agreed within 5.5 % of the NPS system calculated value of 5.5 microns. The agreement between the two light scattering apparatuses was now considered to be excellent.

Prior to the final two rocket firings the two light scattering apparatuses were switched so that the NPS system now measured the internal motor environment and the MALVERN measured the nozzle exhaust. A calibration was conducted on the NPS system using the same procedures and equipment as before, with the exceptions that 9.6 micron polystyrene spheres were used and the sample was measured while sitting in the motor cavity with the nitrogen purge filters and fused silica windows installed. The D_{32} calculated by the NPS system was 9.6 microns (Fig. 4.5).

D. BEAM WANDER

During the course of this investigation beam wander associated with the NPS system measurements of the internal motor environment was not encountered. Several possible causes for the problems reported by Keith [Ref. 9] were discovered. These causes may be grouped into two major catagories: (1) equipment malfunctions, or (2) procedural changes.

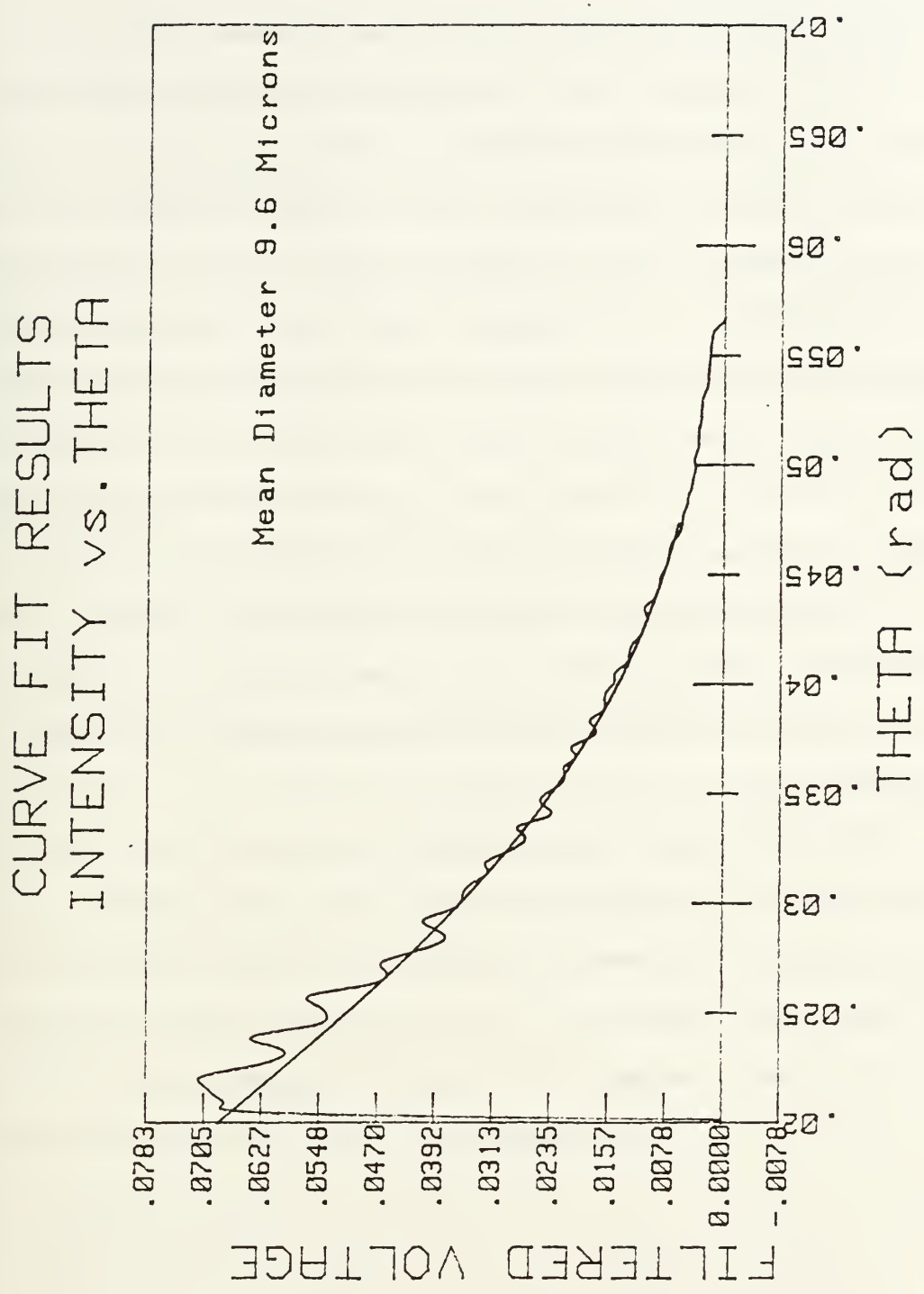

Figure 4.5 Calibration Profile for 9.6 Micron Spheres in Motor Cavity, NPS System

At the beginning of this investigation plans were made to conduct several motor firings using the two NPS light scattering apparatuses used by Keith. The width of the bandpass laser line-filters used in the detector tubes were to be determined and the systems were to be realigned and calibrated prior to firing a rocket motor. During removal of the laser line-filter on the system with which Keith had encountered beam wander the Fourier Transform lens was found to be excessively cocked due to a missing set screw. These lens are held in place by two set screws located 180° apart at the top and bottom of the detector tube. Because of the method of removal of the laser line-filter, it is doubtful that the Fourier Transform lens was cocked during the disassembly.

The function of the Fourier Transform lens is to focus the light to a point based on its angle of incidence on the outer face of the lens. Therefore, if this lens is cocked during system operation, the associated linear diode array will, at best, measure incorrect scattered light intensities for a given angle. The scattered light is focused by the lens in a manner that would provide a ring of light if the particles were monomodal. If the lens is twisted about the axis of the bottom set screw, as well as cocked, then the linear array would not be intersecting these rings along a line normal to the rings. This could, in fact, create stored data of the nature experienced by Keith.

A second problem was encountered with this same system during the calibration phase. Erratic signals from the sample and hold circuit were evident on the oscilloscope during system operation. Over a period of roughly a week the reliability of the circuit worsened and it finally failed completely. Because of the complexity of the sample and hold circuit, no judgement could be made to the possible impact this problem may have had concerning the beam wander experienced by Keith.

Under the second catagory of reasons as to why beam wander was not encountered during this investigation, two procedural differences existed in the use of the NPS system for measuring the internal motor environment. First, measurements were taken at approximately steady propellant chamber pressures (P_c was varying less than 15 psig/second) which would minimize the laser beam deflection resulting from pressure waves mentioned by Keith [Ref. 9]. Secondly, the laser beam diameter was 3-4 times larger than that used by Keith. This should minimize the problem of having the beam move slightly off of the array.

E. MOTOR FIRINGS

The results obtained from the internal motor environment by the MALVERN and presented in this section are based on the data collected by the innermost 28 diode rings.

When the MALVERN was used to sample the nozzle exhaust, all 31 diode rings of collected data were used. This decision was based on the inconsistency of sample results during early rocket motor firings and rough physical measurements obtained from the MALVERN ring array.

Reference 9 illustrates that the maximum angle of scattered light that can freely pass through the window assembly from the motor internals is approximately 6 degrees. The relationship

$$\text{Theta} = \text{Tan}^{-1}(R/X) ,$$

can be used to determine the maximum detectable scattering angle for the MALVERN. R/X can be the ratio of the radius of the associated detector lens to the cutoff distance (as defined in Figure 5.2-B of Reference 11) or the ratio of the diode array heigth to the focal length of the detector lens. Using 6° for Theta and solving for the diode array heigth gives a maximum height of approximately 0.4 inches. This 0.4 inch heigth roughly includes the inner 28 diode rings. Data collected by rings 29-31 are suspected to include light scattered by the window nitrogen purge filter and was excluded during internal motor environment sampling. More accurate information concerning diode ring spacing will be available at the Naval Postgraduate School in the near

future, and the present estimation will be refined in a later investigation.

Table III gives a summary of rocket motor firings and the associated parameters. The tests conducted fell into three basic groups: (1) motor firings with a propellant containing 2% aluminum which were conducted to established a combination of a neutral burning propellant chamber pressure and a sufficiently large particle concentration in the nozzle exhaust to provide reliable sampling by the two systems, (2) motor firings using a propellant with 6 micron diameter zirconium carbide for the purpose of sampling for a known particle size in the motor and nozzle exhaust of a burning rocket motor, and (3) motor firings with a propellant containing 2.0% aluminum with repeatable operational parameters such that verification of measurements could be provided by data obtained during two consecutive firings. In addition, cross validation could be accomplished by repeating the tests with the sampling location of the two light scattering systems switched. The tests listed in Table III will be discussed using these groupings. Experimental results for all firings discussed are summarized in Table IV.

The first group of tests includes those motor firings conducted during 5-7 May and 15-18 May. The test of 5-7 May were conducted using a 0.335 inch graphite nozzle. The 5 May test used a 1.9 inch diameter by 1.25 inch thick end burning

TABLE III

SUMMARY OF MOTOR FIRINGS

Date of Test	Wt. of Metal (%)	Meas Press P_c (psig)	Max Press P_c (psig)	Burn Time (sec)	Prop Surf Area (in^2)	Throat Dia D_{th} (in)
May 5, 1987	2.0 Al	17	18	7.7	2.83	0.335
May 6, 1987	2.0 Al	55	58	4.9	*4.79	0.335
May 7, 1987	2.0 Al	55	56	5.1	*4.79	0.335
May 12, 1987	1.0 ZrC	124	139	7.2	2.83	0.2
May 13, 1987	1.0 ZrC	119	130	6.5	2.83	0.2
May 15, 1987	2.0 Al	42	53	5.8	2.83	0.28
May 18, 1987	2.0 Al	190	273	3.6	2.83	0.2
May 19, 1987	2.0 Al	265	272	3.5	2.83	0.2
May 20, 1987	2.0 Al	238	260	3.4	2.83	0.2
May 22, 1987	2.0 Al	233	241	2.9	2.83	0.2
May 26, 1987	2.0 Al	211	222	3.8	2.83	0.2

NOTE: Propellant surface area indicated by *4.79 represents the same 1.9" propellant diameter, but with the addition of a 0.45" diameter center hole, providing a progressive burn.

TABLE IV

SUMMARY OF EXPERIMENTAL RESULTS

Date of Test	Wt. of Metal (%)	Meas Press (psig)	Burn Time (sec)	Motor D_{32} (microns)	Exhaust D_{32} (microns)
May 5, 1987	2.0 Al	17	7.7	7.0(V) 7.0(N)	N. O.
May 6, 1987	2.0 Al	55	4.9	85.8(V) 7.5(N)	N. O.
May 7,1987	2.0 Al	55	5.1	69.3(V) 64.8(N)	N. O.
May 12, 1987	1.0 ZrC	124	7.2	43.0(V) 27.0(N)	9.5(?)
May 13, 1987	1.0 ZrC	119	6.5	47.7(V) 32.4(N)	6.5(?)
May 19, 1987	2.0 Al	265	3.5	4.3(V) 4.3(N)	6.2
May 20, 1987	2.0 Al	238	3.4	4.3(V) 4.3(N)	4.6
May 22, 1987	2.0 Al	233	2.9	4.4	127.1(V) 122.6(N)
May 26, 1987	2.0 Al	211	3.8	4.6	97.6(V) 1.1(N)

(V) -- MALVERN Volume Distribution D_{32}
(N) -- MALVERN Number Distribution D_{32}
(?) -- faulty diodes at smaller angles

propellant grain while those of 6 and 7 May used a propellant grain of the same dimensions, but with a 0.45 inch center hole added to cause a progressive burn. Neither objective was accomplished with these test. The propellant chamber pressure never reached a plateau during the motor burn and the scattered light intensity was too low to produce usable data for the NPS system (Figure 4.6). At this point in the testing it was felt that a smaller nozzle diameter was required (1) to provide a high enough chamber pressure associated with an end burning propellant grain and (2) to increase the particle concentration in the nozzle exhaust.

The light scattering data obtained by the MALVERN during the 5-7 May testing was, on the other hand, informative. The 5 May low chamber pressure test results shown in Figure 4.7 indicated that the particles inside the motor had a D_{32} of 7.0 microns. On 6 May when the chamber pressure was approximately 3.6 times greater the D_{32} shown in Figure 4.8 increased to 85.8 microns. As propellant chamber pressure increases, burning rate increases as expected (indicated in Table III by the reduction in burn times from 5 to 6 May). With an increased burning rate and higher chamber pressure the metal particles should spend less time on the burning propellant surface, particle agglomeration should decrease and more complete burning of the particles should occur. This should have resulted in the

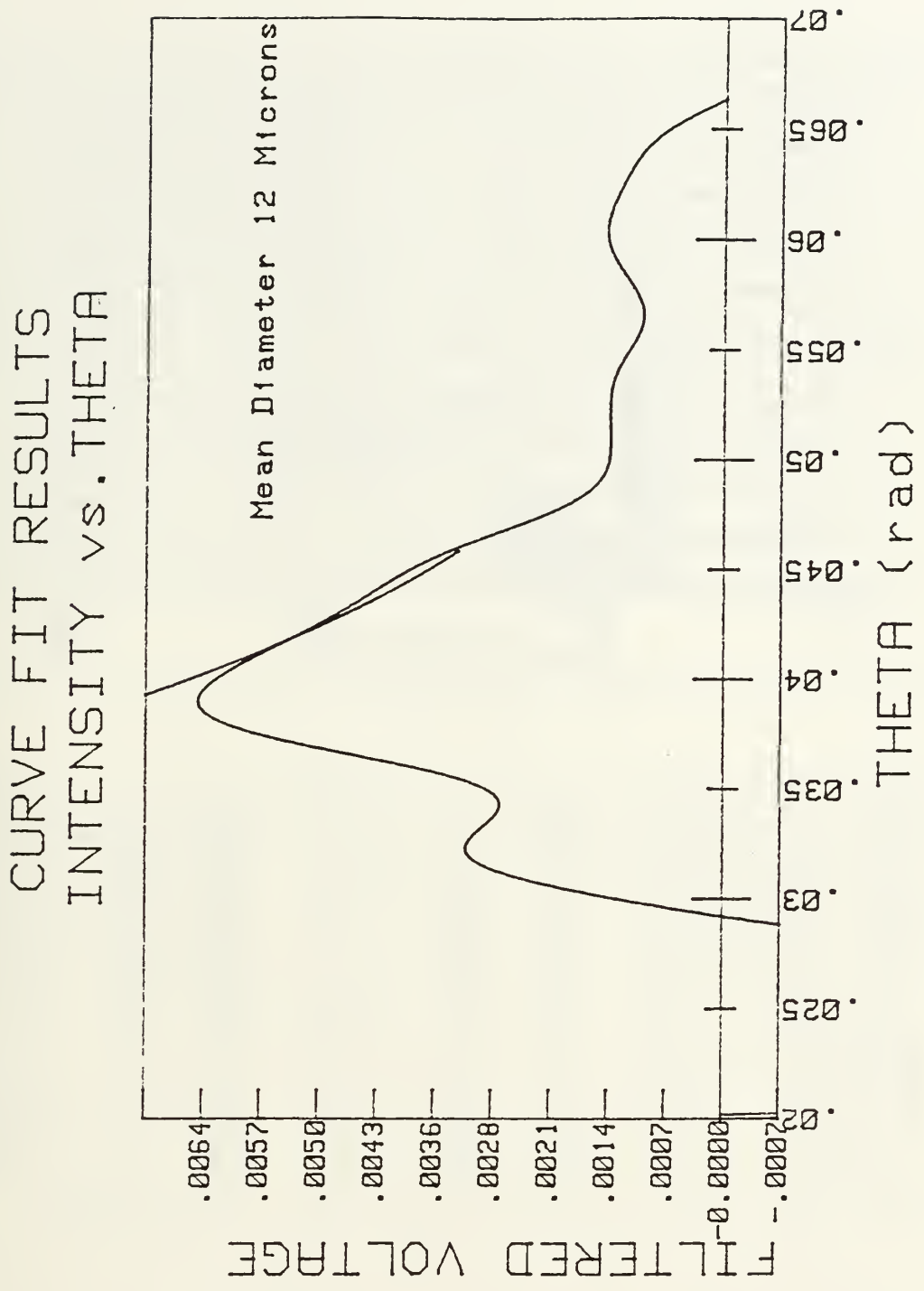

Figure 4.6 Low Voltage Exhaust Profile

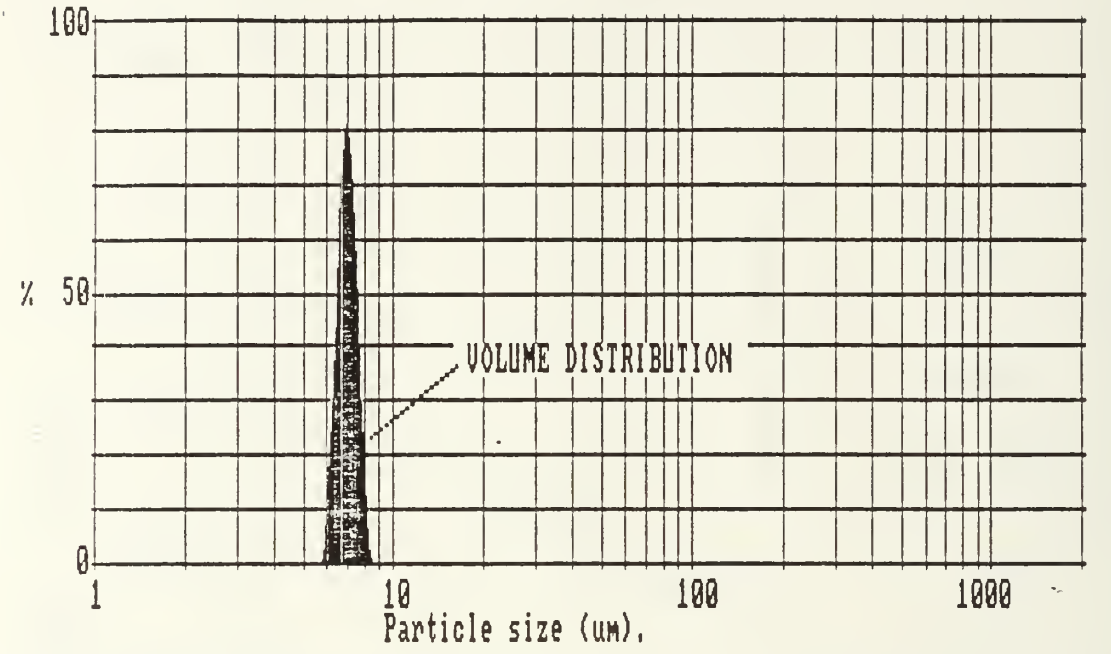

Size microns	under	% in band	Size microns	under	% in band
188.0	100.0	0.0	17.7	100.0	0.0
162.0	100.0	0.0	15.3	100.0	0.0
140.0	100.0	0.0	13.2	100.0	0.0
121.0	100.0	0.0	11.4	100.0	0.0
104.0	100.0	0.0	9.8	100.0	0.0
89.9	100.0	0.0	8.5	100.0	25.3
77.5	100.0	0.0	7.3	74.7	73.3
66.9	100.0	0.0	6.3	1.4	1.4
57.7	100.0	0.0	5.4	0.0	0.0
49.8	100.0	0.0	4.7	0.0	0.0
42.9	100.0	0.0	4.1	0.0	0.0
37.1	100.0	0.0	3.5	0.0	0.0
32.0	100.0	0.0	3.0	0.0	0.0
27.6	100.0	0.0	2.6	0.0	0.0
23.8	100.0	0.0	2.2	0.0	0.0
20.5	100.0	0.0	1.9	0.0	0.0

Result source=testdata
Record No. = 4
Focal length = 100 mm.
Experiment type pia
Volume distribution
Beam length = 51.0 mm.
Obscuration =-.0159
Volume Conc. = 0.0000 %
Log. Diff. =6.53
Model indp

D(v,0.5) = 7.0 µm
D(v,0.9) = 7.5 µm
D(v,0.1) = 6.5 µm
D(4,3) = 7.0 µm
D(3,2) = 7.0 µm
Span = 0.1
Spec. surf. area
0.86 sq.m./cc.

Figure 4.7 Volume Distribution Motor Results Using Inner 28 Diode Rings, 5 May

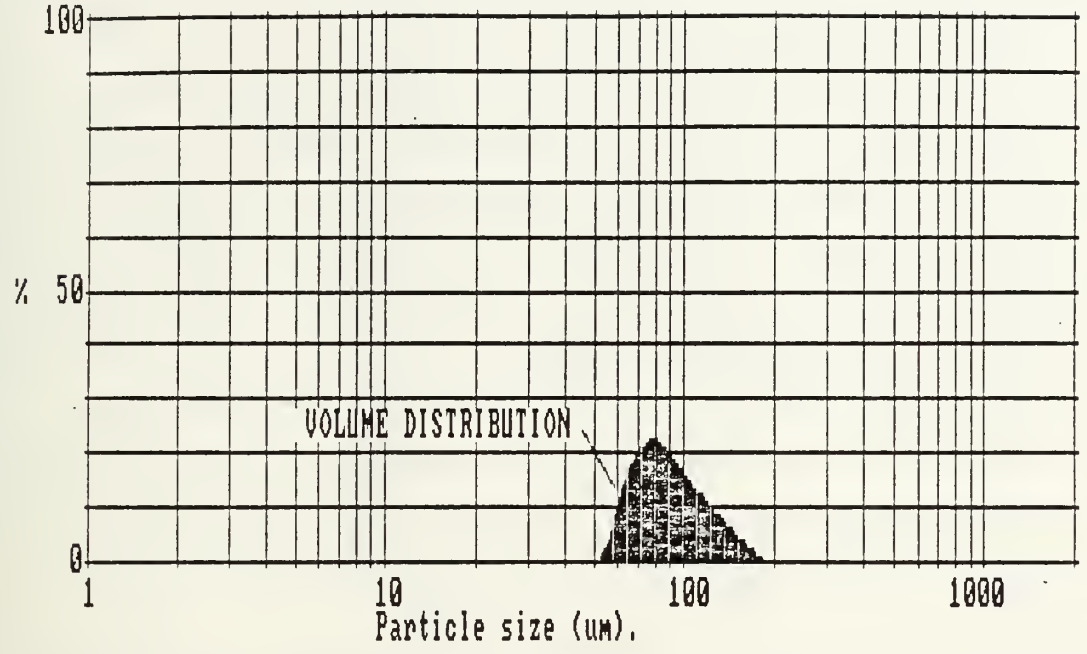

Size microns	under	% in band	Size microns	under	% in band
188.0	100.0	1.5	17.7	0.0	0.0
162.0	98.5	4.7	15.3	0.0	0.0
140.0	93.8	8.2	13.2	0.0	0.0
121.0	85.6	12.7	11.4	0.0	0.0
104.0	73.0	16.6	9.8	0.0	0.0
89.9	56.4	21.1	8.5	0.0	0.0
77.5	35.3	20.4	7.3	0.0	0.0
66.9	14.9	13.1	6.3	0.0	0.0
57.7	1.7	1.7	5.4	0.0	0.0
49.8	0.1	0.0	4.7	0.0	0.0
42.9	0.0	0.0	4.1	0.0	0.0
37.1	0.0	0.0	3.5	0.0	0.0
32.0	0.0	0.0	3.0	0.0	0.0
27.6	0.0	0.0	2.6	0.0	0.0
23.8	0.0	0.0	2.2	0.0	0.0
20.5	0.0	0.0	1.9	0.0	0.0

Result source=testdata
Record No. = 5
Focal length = 100 mm.
Experiment type pia
Volume distribution
Beam length = 51.0 mm.
Obscuration =0.9579
Volume Conc. = 0.1886 %
Log. Diff. =5.52
Model indp

D(v,0.5) = 85.7 µm
D(v,0.9) = 129.7 µm
D(v,0.1) = 64.1 µm
D(4,3) = 92.0 µm
D(3,2) = 85.8 µm
Span = 0.8
Spec. surf. area
0.05 sq.m./cc.

Figure 4.8 Volume Distribution Motor Results Using Inner 28 Diode Rings, 6 May

6 May D_{32} being approximately equal to or less than the 5 May D_{32}.

In an attempt to clarify the unexpected increase in D_{32} the MALVERN's Master Sizer program was used to transform the 5 and 6 May data to numerical distributions, shown in Figures 4.9 and 4.10 respectively. The numerical distribution D_{32}'s were 7.0 and 7.5 microns. These were in far better agreement with pridictions than the volume distribution calculations. The existence of the large 50-188 micron particles had totally biased the calculation of D_{32} when using a volume distribution function. The volume of a sphere increases as the cube of its radius. A 90.0 micron diameter spherical particle would therefore have approximately 5832 times the volume of a 5.0 micron diameter spherical particle. The introduction of less than 0.02% by number of these large diameter particles would therefore totally nullify the accuracy of the measuring apparatus.

The 7 May test results shown in Figures 4.11 and 4.12 were even more heavily biased toward the large diameter particles. The numerical distribution D_{32} of 64.8 microns was only slightly smaller than the volume distribution D_{32} of 69.3 microns. A possible source of this large particle contamination was the RTV used to inhibit and bond the propellant grain into the chamber. On 6 and 7 May a progressive burning propellant grain had been used which exposed additional RTV at the head-in of the center

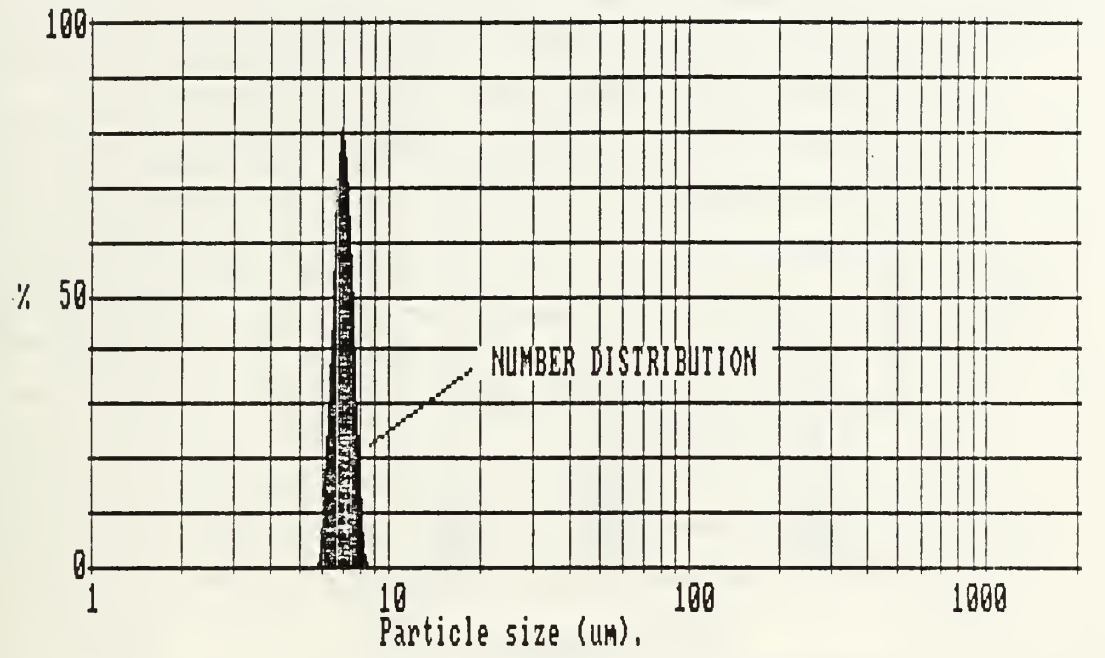

Size microns	under	% in band	Size microns	under	% in band
188.0	100.0	0.0	17.7	100.0	0.0
162.0	100.0	0.0	15.3	100.0	0.0
140.0	100.0	0.0	13.2	100.0	0.0
121.0	100.0	0.0	11.4	100.0	0.0
104.0	100.0	0.0	9.8	100.0	0.0
89.9	100.0	0.0	8.5	100.0	25.3
77.5	100.0	0.0	7.3	74.7	73.3
66.9	100.0	0.0	6.3	1.4	1.4
57.7	100.0	0.0	5.4	0.0	0.0
49.8	100.0	0.0	4.7	0.0	0.0
42.9	100.0	0.0	4.1	0.0	0.0
37.1	100.0	0.0	3.5	0.0	0.0
32.0	100.0	0.0	3.0	0.0	0.0
27.6	100.0	0.0	2.6	0.0	0.0
23.8	100.0	0.0	2.2	0.0	0.0
20.5	100.0	0.0	1.9	0.0	0.0

Result source=testdata
Record No. = 4
Focal length = 100 mm.
Experiment type pia
Number distribution
Beam length = 51.0 mm.
Obscuration =-.0159
Volume Conc. = 0.0000 %
Log. Diff. =6.53
Model indp

D(v,0.5) = 7.0 µm
D(v,0.9) = 7.5 µm
D(v,0.1) = 6.5 µm
D(4,3) = 7.0 µm
D(3,2) = 7.0 µm
Span = 0.1
Spec. surf. area
0.86 sq.m./cc.

Figure 4.9 Number Distribution Motor Results Using Inner 28 Diode Rings, 5 May

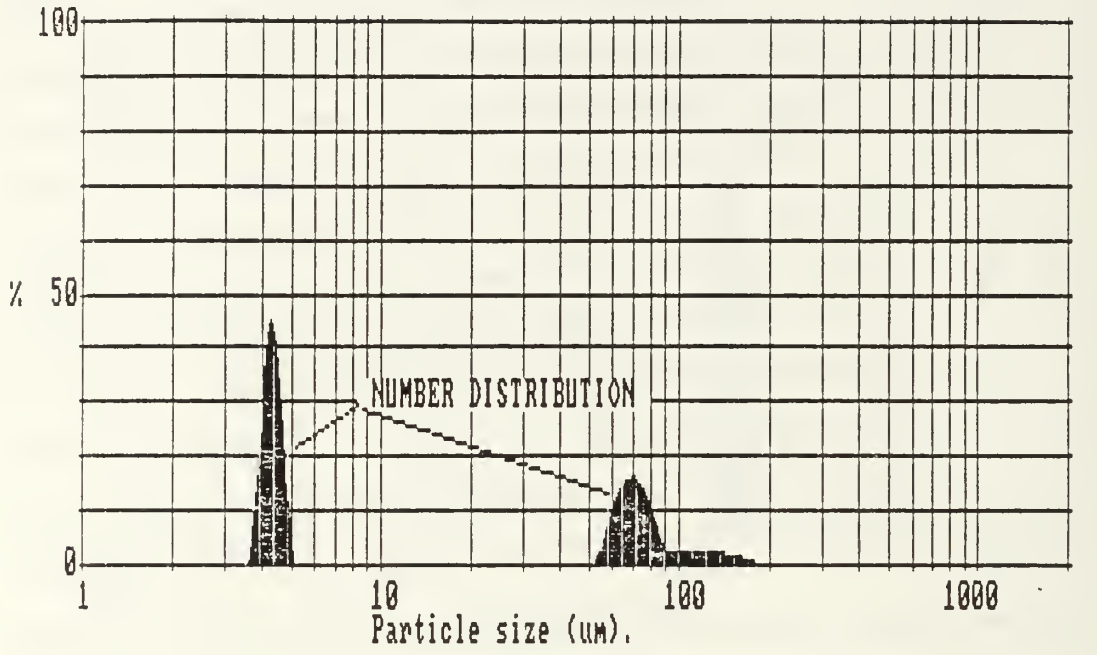

Size microns	under	% in band	Size microns	under	% in band
188.0	100.0	0.7	17.7	54.3	0.0
162.0	99.3	1.6	15.3	54.3	0.0
140.0	97.7	2.2	13.2	54.3	0.0
121.0	95.5	2.4	11.4	54.3	0.0
104.0	93.0	2.0	9.8	54.3	0.0
89.9	91.0	7.3	8.5	54.3	0.0
77.5	83.7	15.2	7.3	54.3	0.0
66.9	68.5	12.5	6.3	54.2	0.0
57.7	56.1	1.8	5.4	54.2	2.8
49.8	54.3	0.0	4.7	51.4	43.6
42.9	54.3	0.0	4.1	7.8	7.9
37.1	54.3	0.0	3.5	0.0	0.0
32.0	54.3	0.0	3.0	0.0	0.0
27.6	54.3	0.0	2.6	0.0	0.0
23.8	54.3	0.0	2.2	0.0	0.0
20.5	54.3	0.0	1.9	0.0	0.0

Result source=testdata
Record No. = 5
Focal length = 100 mm.
Experiment type pia
Number distribution
Beam length = 51.0 mm.
Obscuration =0.9579
Volume Conc. = 0.1886 %
Log. Diff. =5.52
Model indp

D(v,0.5) = 4.7 µm
D(v,0.9) = 85.3 µm
D(v,0.1) = 4.1 µm
D(4,3) = 38.7 µm
D(3,2) = 7.5 µm
Span =17.5
Spec. surf. area
0.05 sq.m./cc.

Figure 4.10 Number Distribution Motor Results Using Inner 28 Diode Rings, 6 May

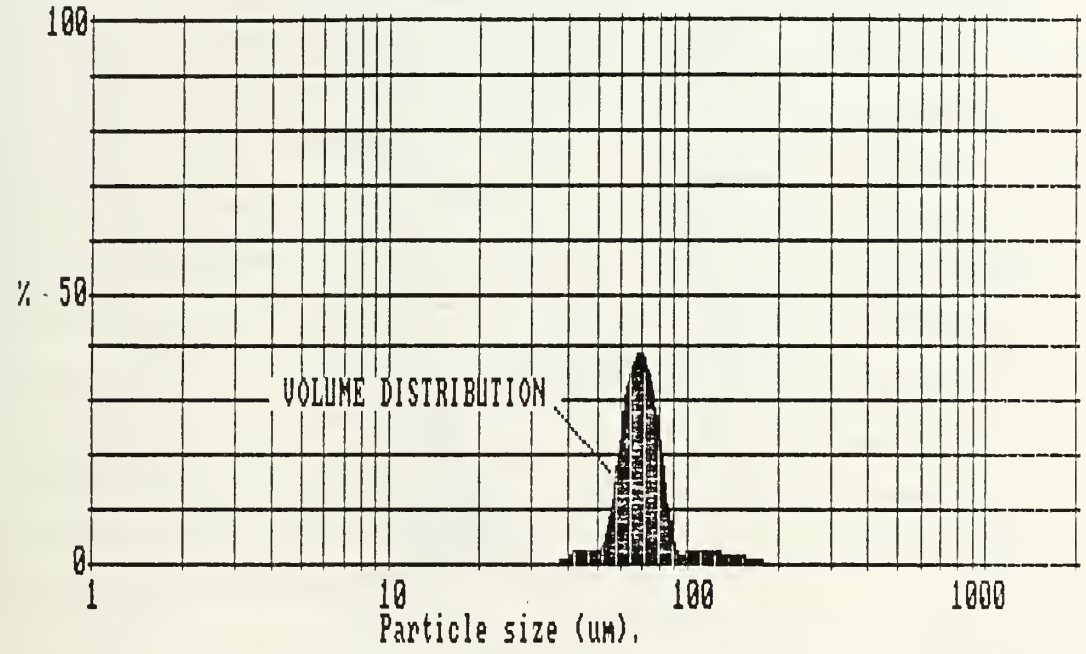

Size microns	under	% in band	Size microns	under	% in band
188.0	100.0	0.5	17.7	0.0	0.0
162.0	99.5	1.3	15.3	0.0	0.0
140.0	98.2	1.8	13.2	0.0	0.0
121.0	96.3	2.2	11.4	0.0	0.0
104.0	94.2	1.8	9.8	0.0	0.0
89.9	92.3	15.8	8.5	0.0	0.0
77.5	76.5	36.7	7.3	0.0	0.0
66.9	39.8	30.4	6.3	0.0	0.0
57.7	9.4	5.5	5.4	0.0	0.0
49.8	3.9	2.5	4.7	0.0	0.0
42.9	1.4	1.4	4.1	0.0	0.0
37.1	0.0	0.0	3.5	0.0	0.0
32.0	0.0	0.0	3.0	0.0	0.0
27.6	0.0	0.0	2.6	0.0	0.0
23.8	0.0	0.0	2.2	0.0	0.0
20.5	0.0	0.0	1.9	0.0	0.0

Result source=testdata
Record No. = 6
Focal length = 100 mm.
Experiment type pia
Volume distribution
Beam length = 51.0 mm.
Obscuration =0.9660
Volume Conc. = 0.1572 %
Log. Diff. =5.32
Model indp

D(v,0.5) = 69.5 µm
D(v,0.9) = 84.5 µm
D(v,0.1) = 58.0 µm
D(4,3) = 72.6 µm
D(3,2) = 69.3 µm
Span = 0.4
Spec. surf. area
0.07 sq.m./cc.

Figure 4.11 Volume Distribution Motor Results Using Inner 28 Diode Rings, 7 May

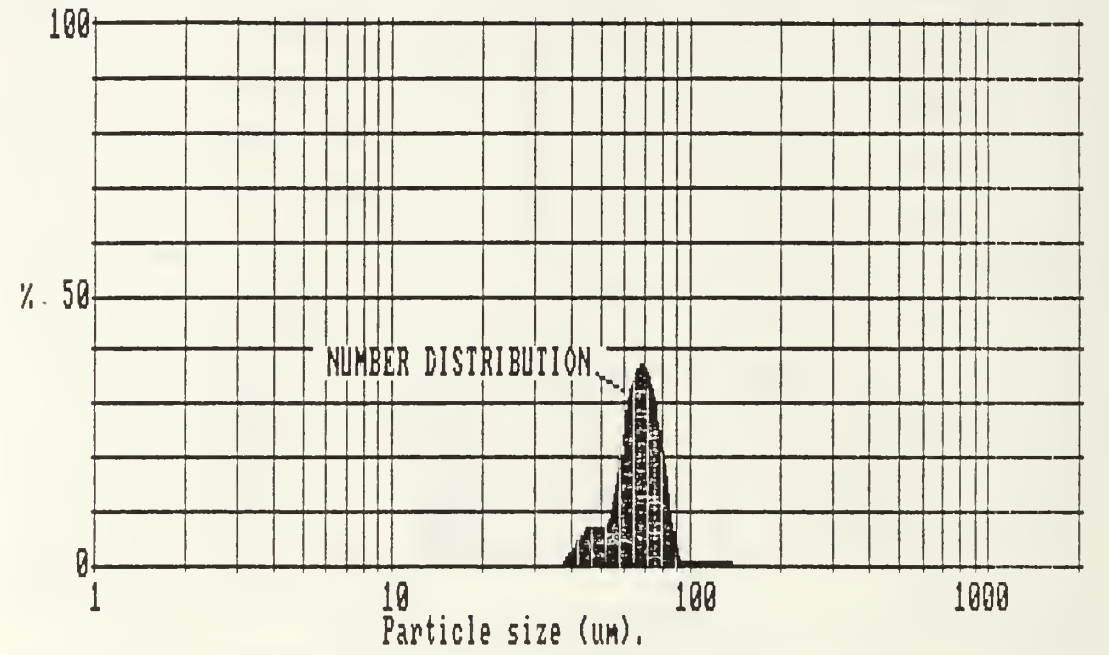

Size microns	under	% in band	Size microns	under	% in band
188.0	100.0	0.1	17.7	0.0	0.0
162.0	99.9	0.3	15.3	0.0	0.0
140.0	99.6	0.4	13.2	0.0	0.0
121.0	99.2	0.7	11.4	0.0	0.0
104.0	98.5	0.6	9.8	0.0	0.0
89.9	97.9	14.1	8.5	0.0	0.0
77.5	83.8	34.7	7.3	0.0	0.0
66.9	49.2	30.4	6.3	0.0	0.0
57.7	18.8	8.9	5.4	0.0	0.0
49.8	9.9	7.0	4.7	0.0	0.0
42.9	2.8	2.8	4.1	0.0	0.0
37.1	0.0	0.0	3.5	0.0	0.0
32.0	0.0	0.0	3.0	0.0	0.0
27.6	0.0	0.0	2.6	0.0	0.0
23.8	0.0	0.0	2.2	0.0	0.0
20.5	0.0	0.0	1.9	0.0	0.0

Result source=testdata
Record No. = 6
Focal length = 100 mm.
Experiment type pia
Number distribution
Beam length = 51.0 mm.
Obscuration =0.9660
Volume Conc. = 0.1572 %
Log. Diff. =5.32
Model indp

D(v,0.5) = 67.1 µm
D(v,0.9) = 80.3 µm
D(v,0.1) = 49.9 µm
D(4,3) = 67.3 µm
D(3,2) = 64.8 µm
Span = 0.5
Spec. surf. area
0.07 sq.m./cc.

Figure 4.12 Number Distribution Motor Results Using Inner 28 Diode Rings, 7 May

perforation to the hot combustion gases throughout the rocket burn. No special testing was conducted to isolate the source of these large particles. However, post-fire motor examinations revealed large quantities of flaking material on the walls.

The tests conducted on 15 and 18 May provided no new information. The data were rough duplicates of those obtained on 6 and 5 May, respectively. Both test indicated the presence of large particles in the range of 50-188 microns. The motor pressure on 18 May settled into a plateau, but the sample was measured while the pressure was still increasing rapidly.

The second test grouping consisted of the test firings on 12 and 13 May. A 0.2 inch diameter graphite nozzle was used in conjunction with an end burning, 1.9 inch diameter by 1.0 inch thick grain of propellant which contained 1.0% zirconium-carbide. The combination of an end burner with a 0.2 inch nozzle produced a flatter pressure trace, shown by Figure 4.13, during motor burn. The 12 and 13 May nozzle exhaust D_{32}'s shown in Figures 4.14 and 4.15 were 9.5 and 6.5 microns respectively. The center portion of these curves from approximately 0.03 to 0.045 radians is low due to several bad diodes being in close proximity in the linear diode array. This resulted in an overestimation of D_{32}. Concentrating on the slope of the curve from 0.045 to 0.065 radians would indicate that a D_{32} of 5-7 microns would be a

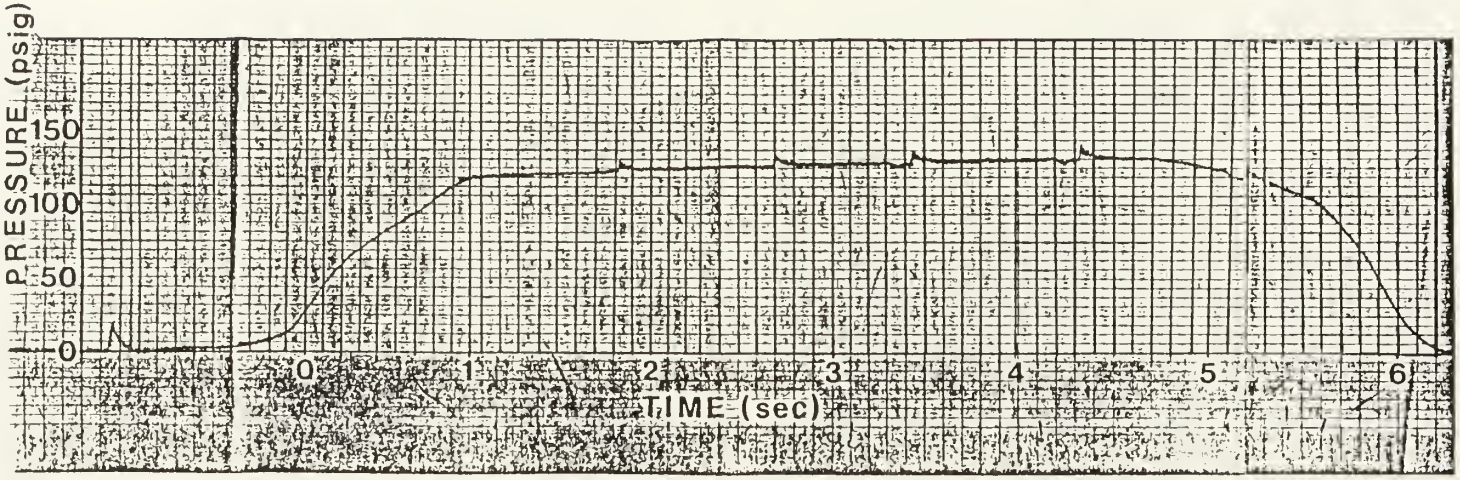

Figure 4.13 Propellant Chamber Pressure, 12 May

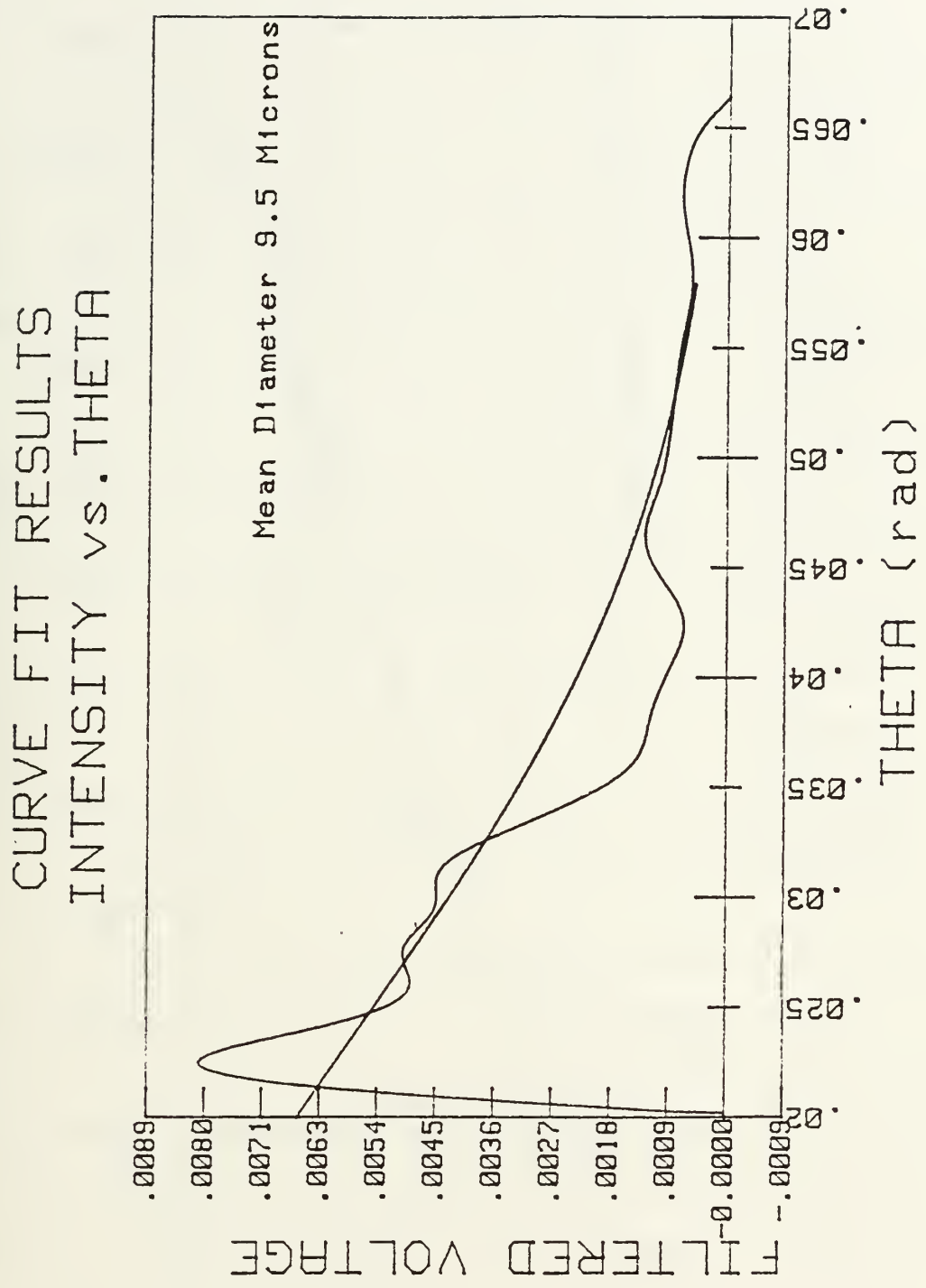

Figure 4.14 Exhaust Profile, 12 May

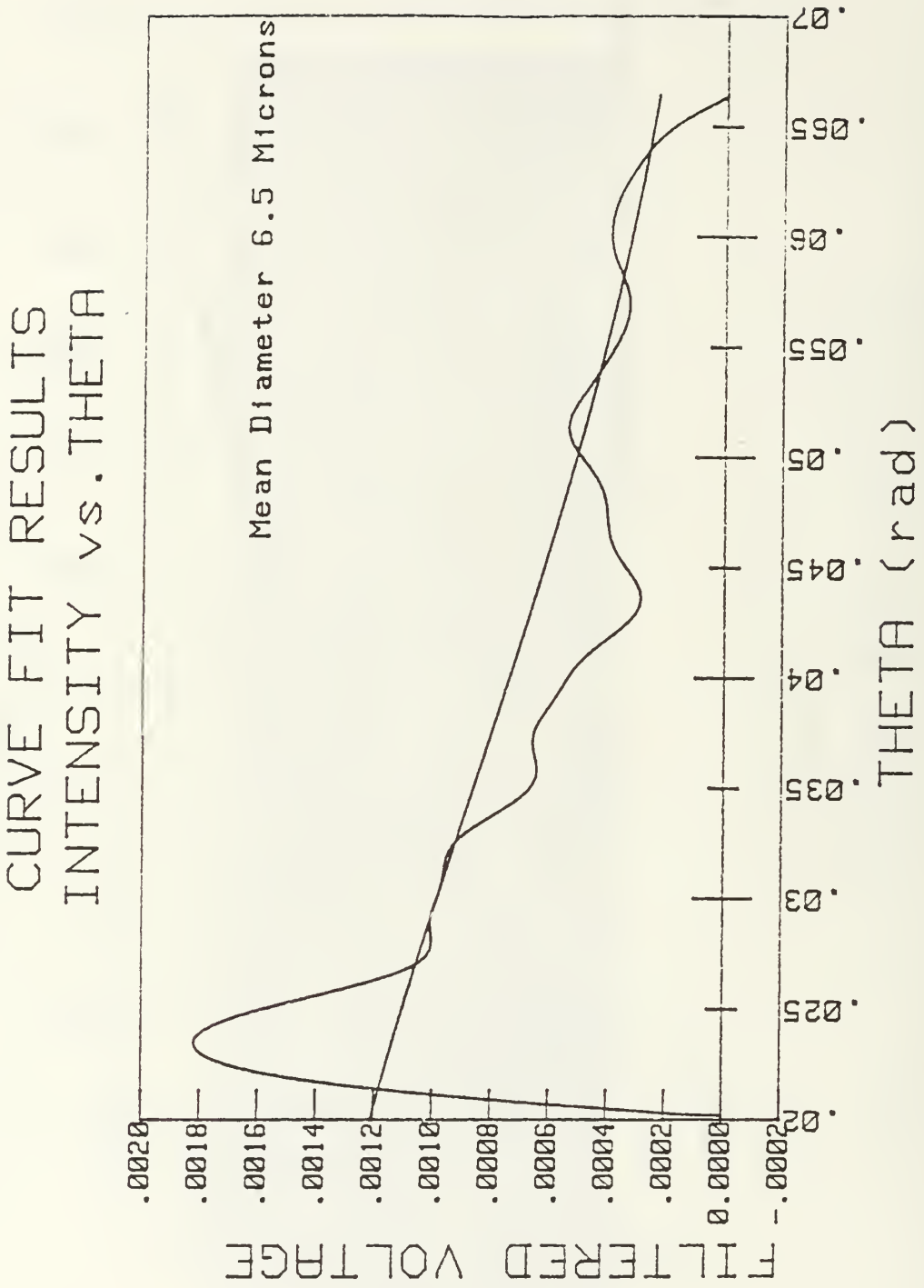

Figure 4.15 Exhaust Profile, 13 May

better estimation. This also represented the expected particle size. In addition, the NPS system was set up to measure small particles. Thus, the minimum detectable scattering angle was currently set at approximately 1.14°. This limits the maximum particle size for accurate measurement to approximately 20 microns, which would greatly reduce any bias toward large particles.

The results of sampling the internal motor environment with the MALVERN are shown in Figures 4.16 through 4.19. The measured D_{32}'s of 27.0 to 47.7 microns were not consistent with the 6 micron zirconium-carbide particles in the burning propellant. Because of the small percentage, by weight, of these particles in the propellant, any contamination by larger particles could totally mask their presence. The RTV material was again suspected of being the source of contamination.

A sample of the 12 May post-fire residue was removed from the motor cavity in the vicinity of the windows (Figure 4.20) and from the converging section of the graphite nozzle (Figures 4.21 and 4.22). These samples were multiple-washed using acetone and then examined using an electron microscope (SEM). The observed spherical particle sizes ranged from 1-20 microns. This is a reasonable size range for a powder mean diameter of 6 microns, and does not support the 27.0 to 47.7 microns measured by the MALVERN. The SEM did indicate

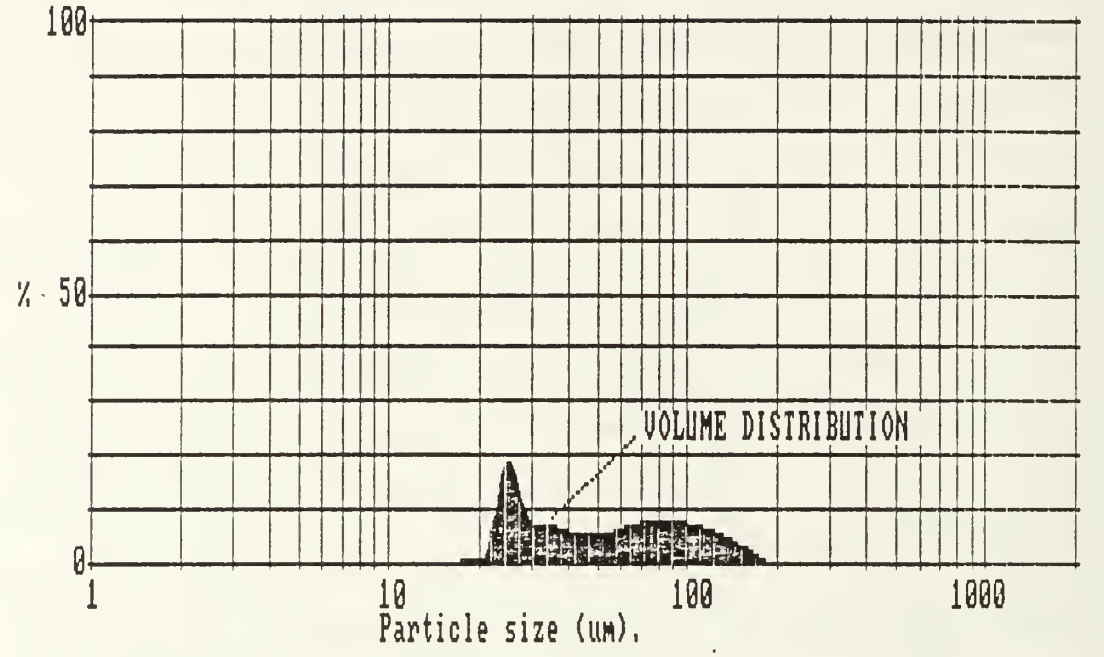

Size microns	under	% in band	Size microns	under	% in band
188.0	100.0	1.3	17.7	0.2	0.2
162.0	98.7	3.4	15.3	0.0	0.0
140.0	95.4	5.1	13.2	0.0	0.0
121.0	90.3	6.6	11.4	0.0	0.0
104.0	83.8	7.1	9.8	0.0	0.0
89.9	76.6	7.6	8.5	0.0	0.0
77.5	69.1	7.3	7.3	0.0	0.0
66.9	61.8	6.5	6.3	0.0	0.0
57.7	55.3	5.2	5.4	0.0	0.0
49.8	50.0	5.0	4.7	0.0	0.0
42.9	45.1	5.6	4.1	0.0	0.0
37.1	39.5	6.9	3.5	0.0	0.0
32.0	32.6	7.2	3.0	0.0	0.0
27.6	25.4	18.0	2.6	0.0	0.0
23.8	7.3	6.3	2.2	0.0	0.0
20.5	1.0	0.8	1.9	0.0	0.0

Result source=testdata
Record No. = 8
Focal length = 100 mm.
Experiment type pia
Volume distribution
Beam length = 51.0 mm.
Obscuration =0.9864
Volume Conc. = 0.1236 %
Log. Diff. =6.10
Model indp

D(v,0.5) = 49.8 µm
D(v,0.9) = 120.1 µm
D(v,0.1) = 24.3 µm
D(4,3) = 61.8 µm
D(3,2) = 43.0 µm
Span = 1.9
Spec. surf. area
0.06 sq.m./cc.

Figure 4.16 Volume Distribution Motor Results Using Inner 28 Diode Rings, 12 May

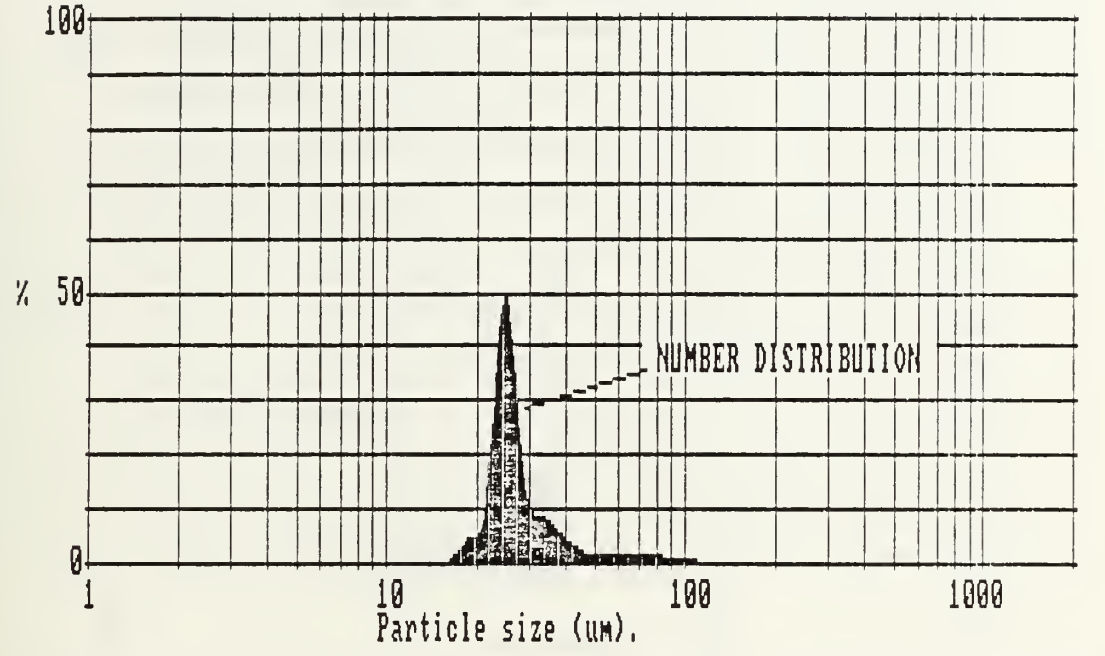

Size microns	under	% in band	Size microns	under	% in band
188.0	100.0	0.0	17.7	1.0	1.0
162.0	100.0	0.0	15.3	0.0	0.0
140.0	100.0	0.1	13.2	0.0	0.0
121.0	99.9	0.4	11.4	0.0	0.0
104.0	99.5	0.7	9.8	0.0	0.0
89.9	98.8	1.1	8.5	0.0	0.0
77.5	97.7	1.4	7.3	0.0	0.0
66.9	96.3	1.4	6.3	0.0	0.0
57.7	94.9	1.3	5.4	0.0	0.0
49.8	93.6	1.9	4.7	0.0	0.0
42.9	91.7	4.4	4.1	0.0	0.0
37.1	87.3	7.8	3.5	0.0	0.0
32.0	79.5	9.6	3.0	0.0	0.0
27.6	69.9	45.4	2.6	0.0	0.0
23.8	24.5	19.0	2.2	0.0	0.0
20.5	5.5	4.5	1.9	0.0	0.0

Result source=testdata
Record No. = 8
Focal length = 100 mm.
Experiment type pia
Number distribution
Beam length = 51.0 mm.
Obscuration =0.9864
Volume Conc. = 0.1236 %
Log. Diff. =6.10
Model indp

D(v,0.5) = 25.6 µm
D(v,0.9) = 40.0 µm
D(v,0.1) = 22.4 µm
D(4,3) = 29.9 µm
D(3,2) = 27.0 µm
Span = 0.7
Spec. surf. area
0.06 sq.m./cc.

Figure 4.17 Number Distribution Motor Results Using Inner 28 Diode Rings, 12 May

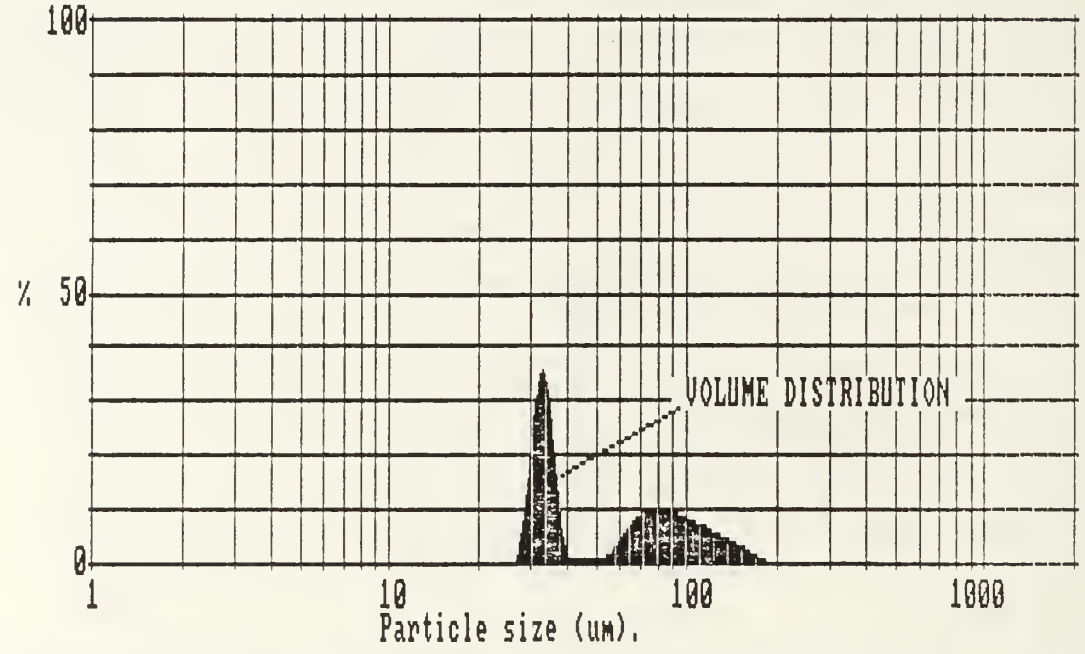

Size microns	under	% in band	Size microns	under	% in band	
188.0	100.0	1.0	17.7	0.0	0.0	Result source=testdata
162.0	99.0	3.0	15.3	0.0	0.0	Record No. = 9
140.0	96.0	4.8	13.2	0.0	0.0	Focal length = 100 mm.
121.0	91.1	6.9	11.4	0.0	0.0	Experiment type pia
104.0	84.3	8.3	9.8	0.0	0.0	Volume distribution
89.9	76.0	9.8	8.5	0.0	0.0	Beam length = 51.0 mm.
77.5	66.2	9.1	7.3	0.0	0.0	Obscuration =0.9668
66.9	57.1	5.9	6.3	0.0	0.0	Volume Conc. = 0.1086 %
57.7	51.2	1.1	5.4	0.0	0.0	Log. Diff. =5.94
49.8	50.1	0.5	4.7	0.0	0.0	Model indp
42.9	49.5	1.3	4.1	0.0	0.0	
37.1	48.3	30.2	3.5	0.0	0.0	D(v,0.5) = 48.7 µm
32.0	18.1	17.9	3.0	0.0	0.0	D(v,0.9) = 117.7 µm
27.6	0.2	0.2	2.6	0.0	0.0	D(v,0.1) = 30.9 µm
23.8	0.1	0.1	2.2	0.0	0.0	D(4,3) = 63.9 µm
20.5	0.0	0.0	1.9	0.0	0.0	D(3,2) = 47.7 µm
						Span = 1.8
						Spec. surf. area
						0.06 sq.m./cc.

Figure 4.18 Volume Distribution Motor Results Using Inner 28 Diode Rings, 13 May

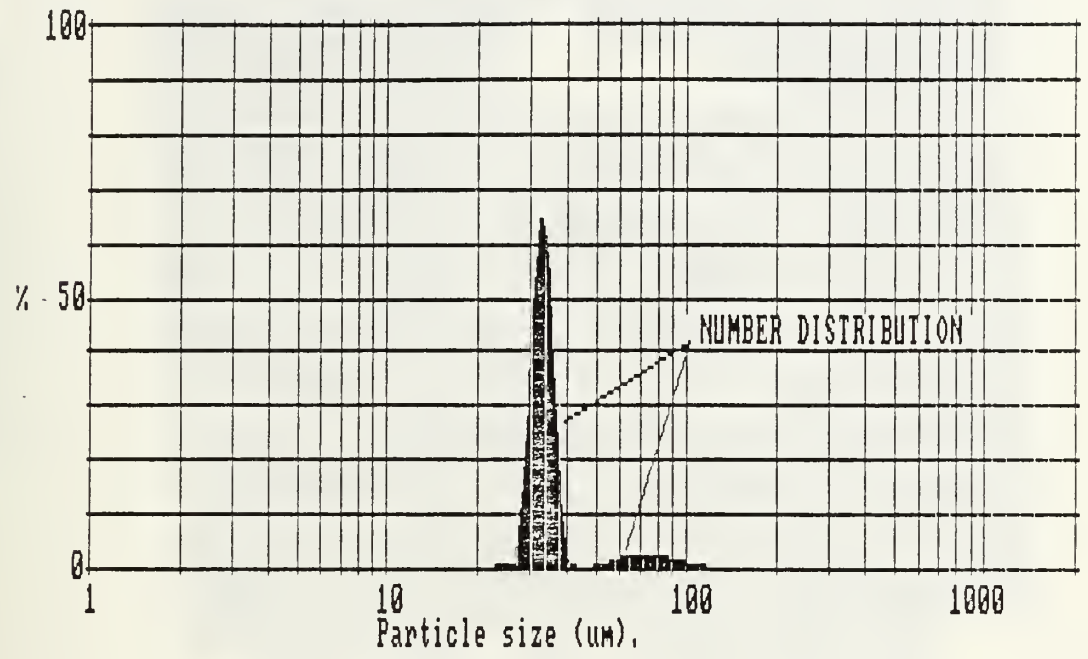

Size microns	under	% in band	Size microns	under	% in band
188.0	100.0	0.0	17.7	0.0	0.0
162.0	100.0	0.0	15.3	0.0	0.0
140.0	100.0	0.0	13.2	0.0	0.0
121.0	100.0	0.6	11.4	0.0	0.0
104.0	99.4	1.3	9.8	0.0	0.0
89.9	98.2	2.2	8.5	0.0	0.0
77.5	96.0	2.5	7.3	0.0	0.0
66.9	93.5	2.1	6.3	0.0	0.0
57.7	91.4	1.0	5.4	0.0	0.0
49.8	90.3	0.3	4.7	0.0	0.0
42.9	90.0	1.6	4.1	0.0	0.0
37.1	88.4	54.8	3.5	0.0	0.0
32.0	33.7	32.8	3.0	0.0	0.0
27.6	0.9	0.6	2.6	0.0	0.0
23.8	0.3	0.3	2.2	0.0	0.0
20.5	0.0	0.0	1.9	0.0	0.0

Result source=testdata
Record No. = 9
Focal length = 100 mm.
Experiment type pia
Number distribution
Beam length = 51.0 mm.
Obscuration =0.9668
Volume Conc. = 0.1086 %
Log. Diff. =5.94
Model indp

D(v,0.5) = 33.1 µm
D(v,0.9) = 42.3 µm
D(v,0.1) = 30.1 µm
D(4,3) = 35.2 µm
D(3,2) = 32.4 µm
Span = 0.4
Spec. surf. area
0.06 sq.m./cc.

Figure 4.19 Number Distribution Motor Results Using Inner 28 Diode Rings, 13 May

Figure 4.20 SEM Photograph of Collected Combustion Products Near Windows, 1.0% ZrC

Figure 4.21 SEM Photograph of Collected Combustion Products In Graphite Nozzle, 1.0% ZrC

Figure 4.22 SEM Photograph of Collected Conbustion Products In Graphite Nozzle, 1.0% ZrC

the presence of large irregular shaped particles, but their source could not be determined.

The Visicorder trace of the chamber pressure for both tests indicated a series of random short pressure spikes. During the 12 May test a KODAK Ektapro high speed video camera recorder (VCR) was used to monitor the nozzle exhaust. At a speed of 1000 frames per second this VCR was able to visually capture the sequence that occurred. Refering to Figure 4.23 (viewing from top to bottom) the following events are indicated: (1) normal exhaust flow with the scattered laser beam visible just to the right of the point of the bright area, (2) three milliseconds later, pressure upstream of the nozzle throat has increased causing a much greater rate of expansion of the exhaust gases at the nozzle outlet, and (3) twelve milliseconds after the pressure flareup started, a residue of large particle sizes was blown free of the nozzle with the scattered laser beam now evident at the right lower side of the bright area and partially blocked from view by what appears to be a large clump of material that has broken free of the nozzle.

These VCR prints provided additional proof that large particle sizes were, in fact, being produced in the internal motor environment. Data had now been obtained by two totally independent methods to support this fact. In addition (as mentioned above), after firing a motor, the propellant chamber walls were covered by a large flaky material that

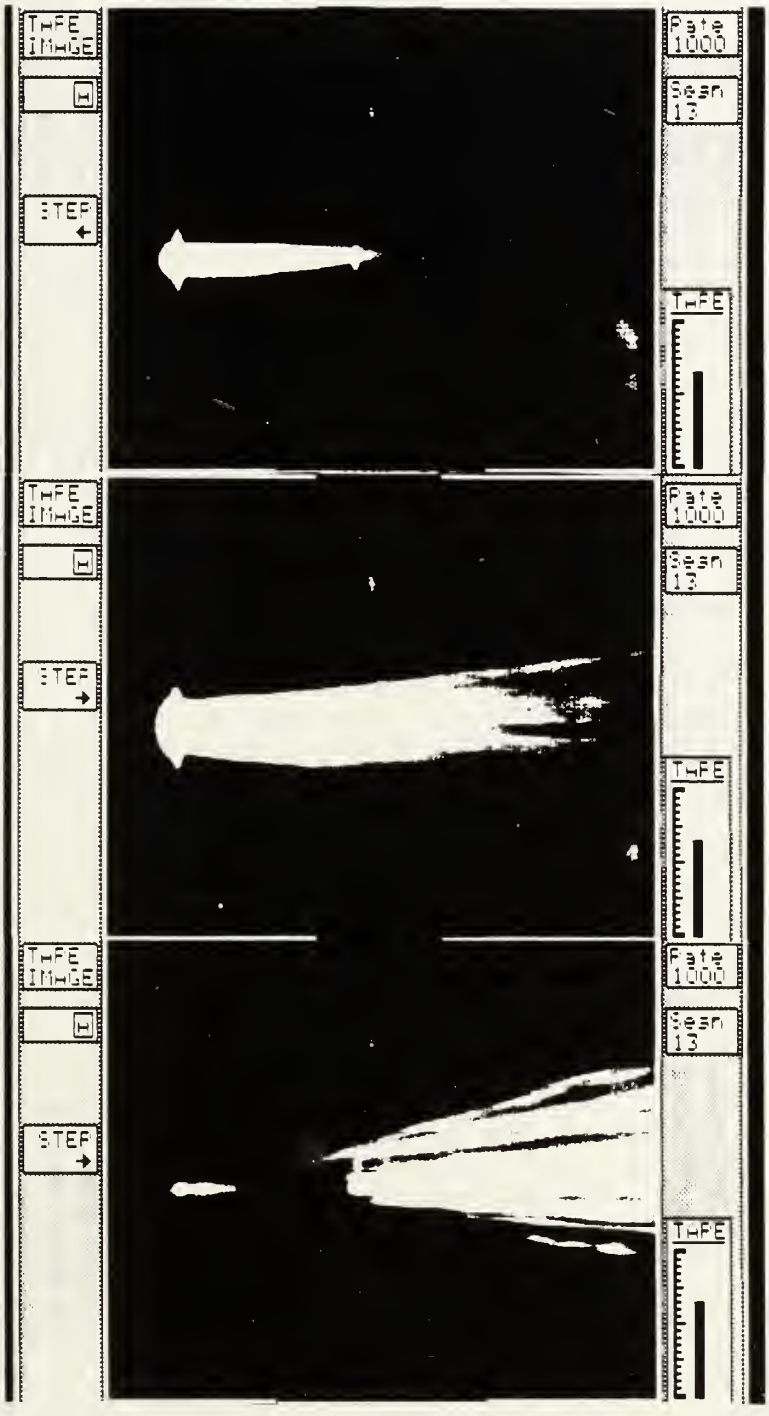

Figure 4.23 High Speed VCR Prints of Partial Nozzle Blockage

rapidy dissipated as the distance from the bonded surface increased. Because two completely different propellants were used during the tests, but the same bonding material was used with both propellants, the RTV was the most likely source of the large particle contamination.

The third group of tests were those conducted during 19-26 May. A 0.2 inch diameter graphite nozzle was used with an end burning 1.9 inch diameter by 1.0 inch thick grain of 2.0% aluminized propellant. The light scattering measurements were taken on the pressure plateau at 92% and 97% of maximum chamber pressure, with burn times ranging from 2.9 to 3.8 seconds. The purpose of these tests was to first ensure that the data obtained by the two light scattering apparatuses would repeat, given the same set of conditions. Secondly, the two systems were interchanged as another method of checking how well the analyzed data would correlate between the two systems.

The effect of the bad diodes on the linear array together with low scattered light intensities resulted in distorted scattering profiles near .035 radians. Background light-noise was also limited almost entirely to less than .035 radians. The decision was therefore made to eliminate the subtraction of the background data by the program. This was accomplished by modifying line 1470 of the RDC1 program as listed in the appendix of Reference 7 to read

1470 MAT Av1=Av2 .

The NPS scattered light profiles used in this chapter for the tests of 19-26 May therefore, include the small background noise.

On 19 May, the D_{32} measured by the NPS system at the nozzle exhaust (Figure 4.24) was approximately 6.2 microns. On 20 May the NPS system measured a D_{32} of 4.6 microns (Figure 4.25). On the same dates, the MALVERN 2600 measured internal motor environment D_{32}'s of 4.3 microns (Figures 4.26-4.29) based on both volume and number.

A sample of the 19 May post-fire residue was removed from the converging section of the graphite nozzle. SEM photographs (Figure 4.30-4.32) of the residue displayed spherical particle sizes ranging from less than 1.0 to greater than 30 microns. Large irregular shaped particles similiar to those viewed in the 12 May samples (Figures 4.20-4.22) were also present in large numbers.

The MALVERN and NPS systems were then switched so that the NPS system would measure in the internal motor environment and the MALVERN would measure in the nozzle exhaust. The calibration of the NPS system was verified using 9.6 micron particles as discussed earlier. Then on 22 and 26 May the test conditions of 19 and 20 May were repeated.

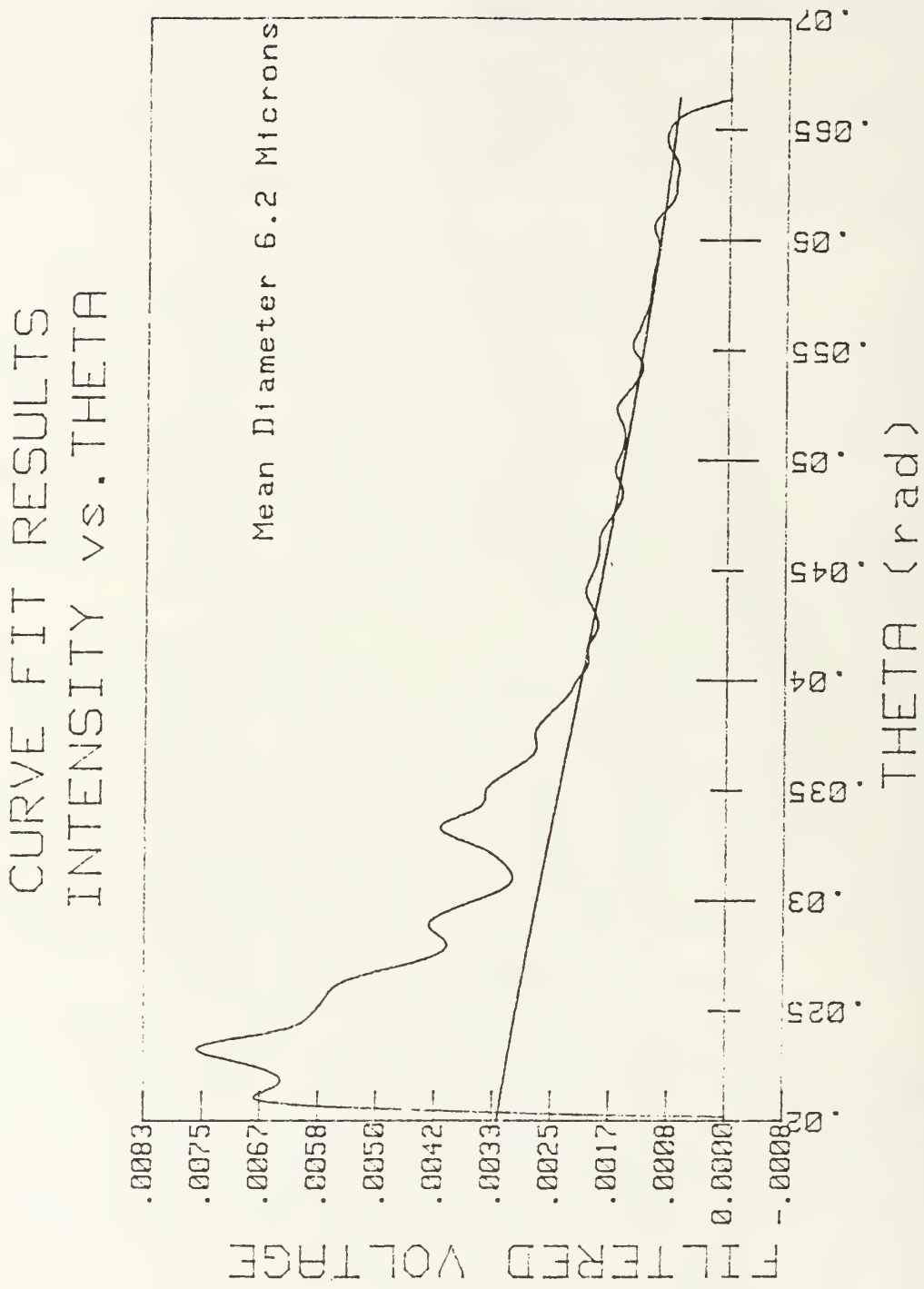

Figure 4.24 Exhaust Profile, 19 May

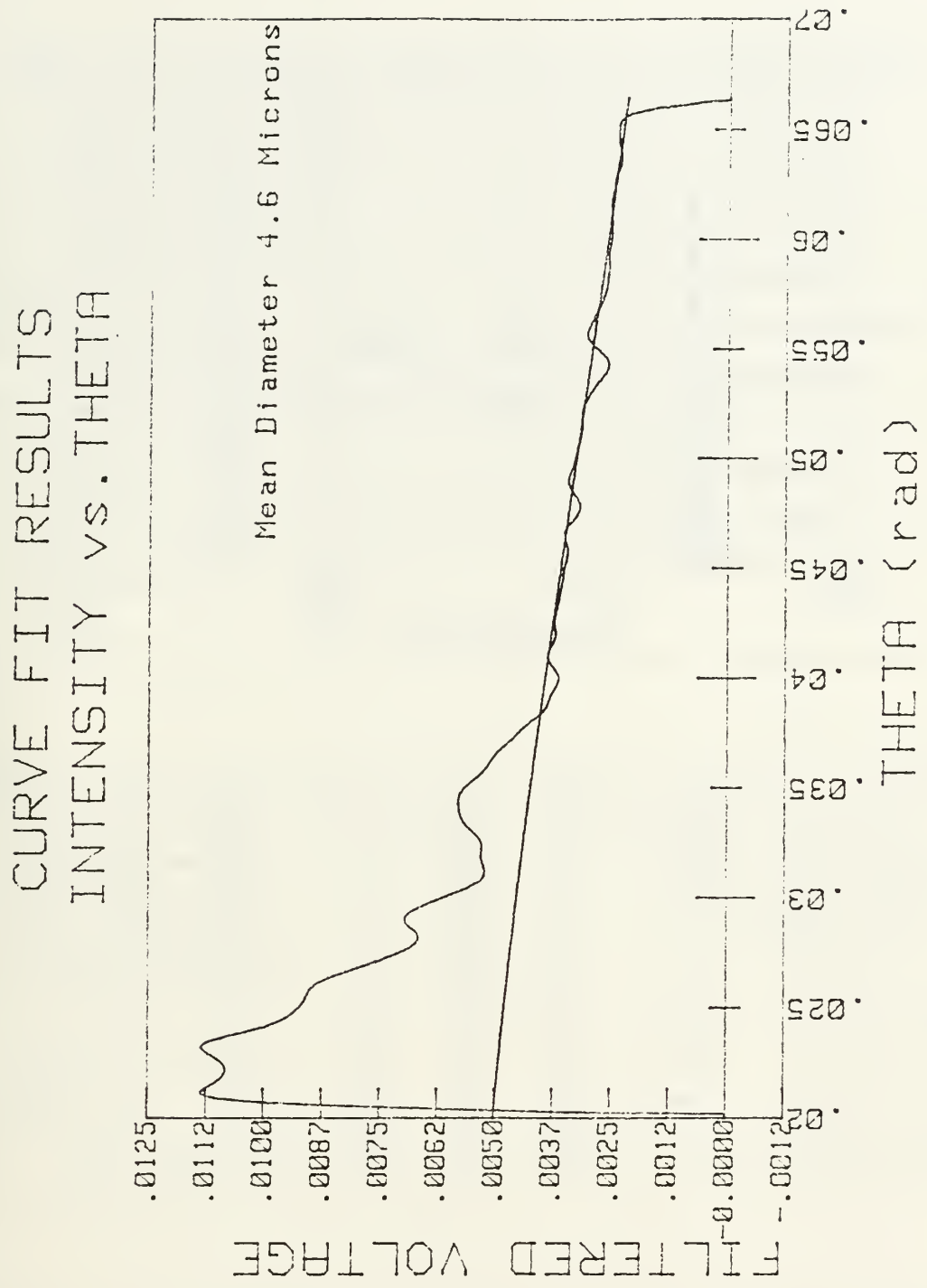

Figure 4.25 Exhaust Profile, 20 May

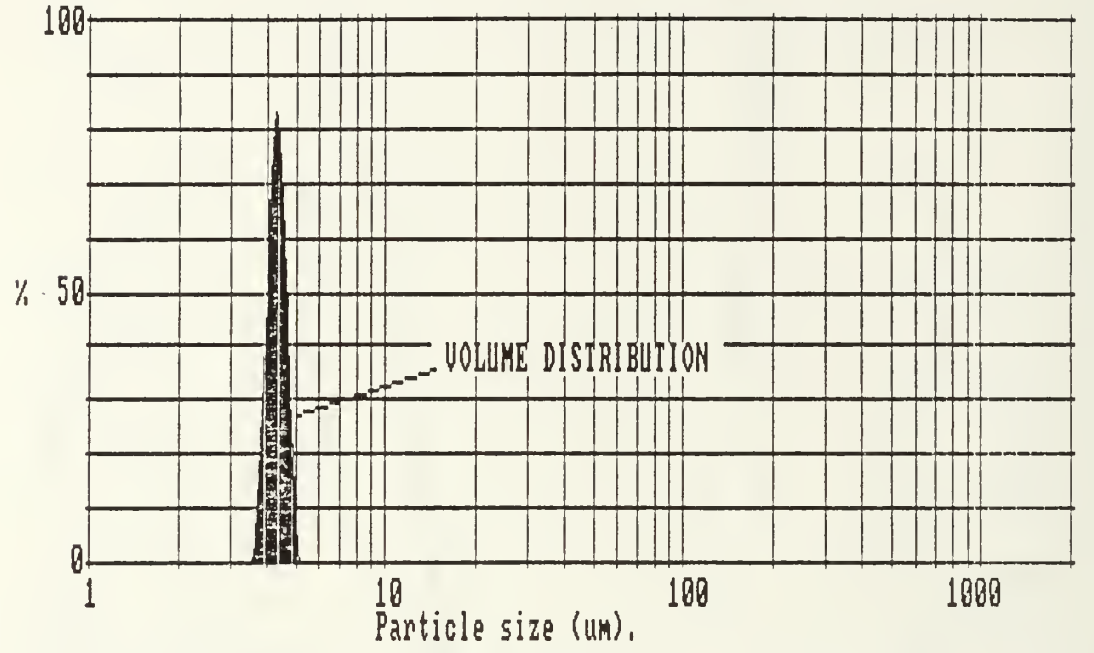

Size microns	under	% in band	Size microns	under	% in band
188.0	100.0	0.0	17.7	100.0	0.0
162.0	100.0	0.0	15.3	100.0	0.0
140.0	100.0	0.0	13.2	100.0	0.0
121.0	100.0	0.0	11.4	100.0	0.0
104.0	100.0	0.0	9.8	100.0	0.0
89.9	100.0	0.0	8.5	100.0	0.0
77.5	100.0	0.0	7.3	100.0	0.0
66.9	100.0	0.0	6.3	100.0	0.0
57.7	100.0	0.0	5.4	100.0	5.0
49.8	100.0	0.0	4.7	94.9	80.3
42.9	100.0	0.0	4.1	14.6	14.6
37.1	100.0	0.0	3.5	0.0	0.0
32.0	100.0	0.0	3.0	0.0	0.0
27.6	100.0	0.0	2.6	0.0	0.0
23.8	100.0	0.0	2.2	0.0	0.0
20.5	100.0	0.0	1.9	0.0	0.0

Result source=testdata
Record No. = 13
Focal length = 100 mm.
Experiment type pia
Volume distribution
Beam length = 51.0 mm.
Obscuration =0.0407
Volume Conc. = 0.0001 %
Log. Diff. =6.62
Model indp

D(v,0.5) = 4.3 µm
D(v,0.9) = 4.6 µm
D(v,0.1) = 4.0 µm
D(4,3) = 4.3 µm
D(3,2) = 4.3 µm
Span = 0.1
Spec. surf. area
1.40 sq.m./cc.

Figure 4.26 Volume Distribution Motor Results Using Inner 28 Diode Rings, 19 May

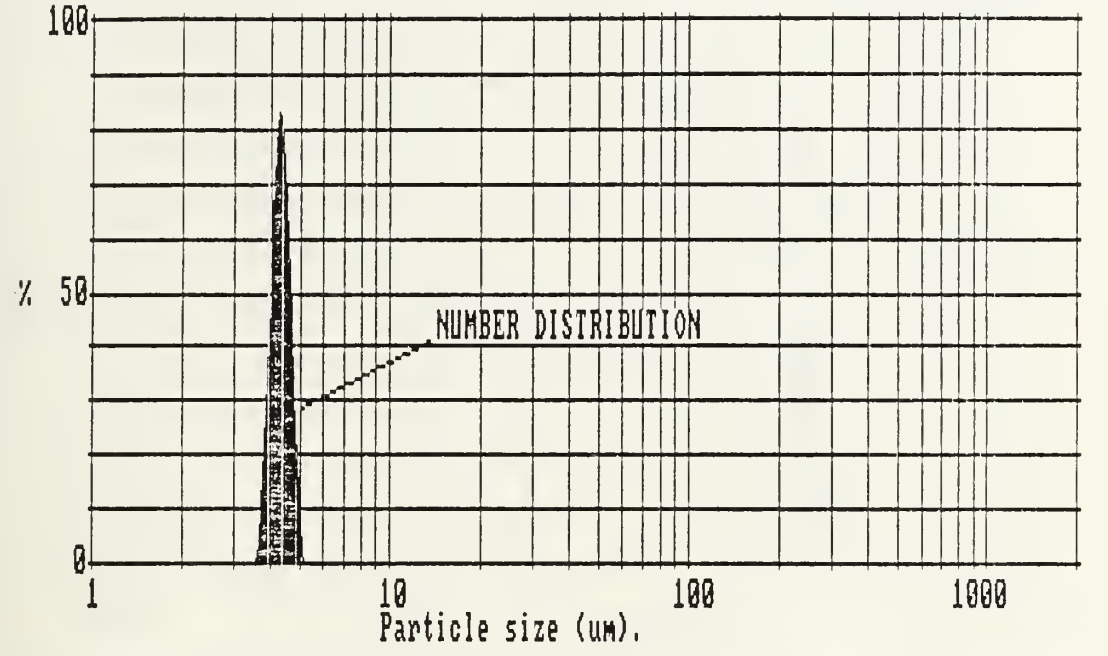

Size microns	under	% in band	Size microns	under	% in band
188.0	100.0	0.0	17.7	100.0	0.0
162.0	100.0	0.0	15.3	100.0	0.0
140.0	100.0	0.0	13.2	100.0	0.0
121.0	100.0	0.0	11.4	100.0	0.0
104.0	100.0	0.0	9.8	100.0	0.0
89.9	100.0	0.0	8.5	100.0	0.0
77.5	100.0	0.0	7.3	100.0	0.0
66.9	100.0	0.0	6.3	100.0	0.0
57.7	100.0	0.0	5.4	100.0	5.0
49.8	100.0	0.0	4.7	94.9	80.3
42.9	100.0	0.0	4.1	14.6	14.6
37.1	100.0	0.0	3.5	0.0	0.0
32.0	100.0	0.0	3.0	0.0	0.0
27.6	100.0	0.0	2.6	0.0	0.0
23.8	100.0	0.0	2.2	0.0	0.0
20.5	100.0	0.0	1.9	0.0	0.0

Result source=testdata
Record No. = 13
Focal length = 100 mm.
Experiment type pia
Number distribution
Beam length = 51.0 mm.
Obscuration =0.0407
Volume Conc. = 0.0001 %
Log. Diff. =6.62
Model indp

D(v,0.5) = 4.3 µm
D(v,0.9) = 4.6 µm
D(v,0.1) = 4.0 µm
D(4,3) = 4.3 µm
D(3,2) = 4.3 µm
Span = 0.1
Spec. surf. area
1.40 sq.m./cc.

Figure 4.27 Number Distribution Motor Results Using Inner 28 Diode Rings, 19 May

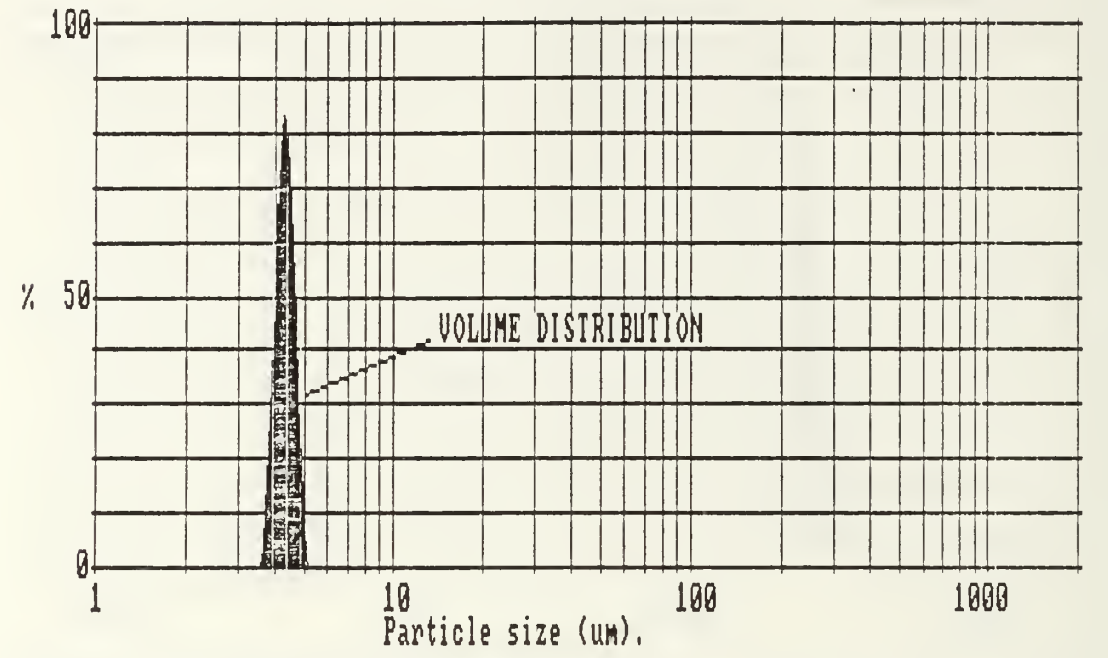

Size microns	under	% in band	Size microns	under	% in band
188.0	100.0	0.0	17.7	100.0	0.0
162.0	100.0	0.0	15.3	100.0	0.0
140.0	100.0	0.0	13.2	100.0	0.0
121.0	100.0	0.0	11.4	100.0	0.0
104.0	100.0	0.0	9.8	100.0	0.0
89.9	100.0	0.0	8.5	100.0	0.0
77.5	100.0	0.0	7.3	100.0	0.0
66.9	100.0	0.0	6.3	100.0	0.0
57.7	100.0	0.0	5.4	100.0	5.0
49.8	100.0	0.0	4.7	94.9	80.3
42.9	100.0	0.0	4.1	14.6	14.6
37.1	100.0	0.0	3.5	0.0	0.0
32.0	100.0	0.0	3.0	0.0	0.0
27.6	100.0	0.0	2.6	0.0	0.0
23.8	100.0	0.0	2.2	0.0	0.0
20.5	100.0	0.0	1.9	0.0	0.0

Result source=testdata
Record No. = 14
Focal length = 100 mm.
Experiment type pia
Volume distribution
Beam length = 51.0 mm.
Obscuration =0.9892
Volume Conc. = 0.0128 %
Log. Diff. =5.44
Model indp

D(v,0.5) = 4.3 µm
D(v,0.9) = 4.6 µm
D(v,0.1) = 4.0 µm
D(4,3) = 4.3 µm
D(3,2) = 4.3 µm
Span = 0.1
Spec. surf. area
1.40 sq.m./cc.

Figure 4.28 Volume Distribution Motor Results Using Inner 28 Diode Rings, 20 May

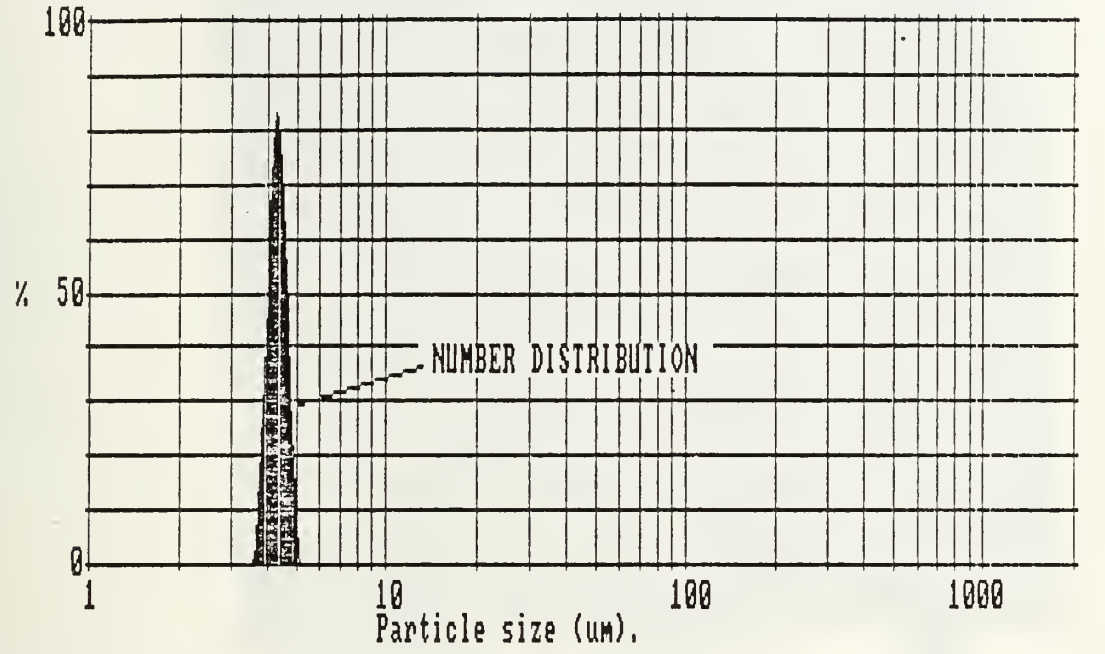

Size microns	under	% in band	Size microns	under	% in band
188.0	100.0	0.0	17.7	100.0	0.0
162.0	100.0	0.0	15.3	100.0	0.0
140.0	100.0	0.0	13.2	100.0	0.0
121.0	100.0	0.0	11.4	100.0	0.0
104.0	100.0	0.0	9.8	100.0	0.0
89.9	100.0	0.0	8.5	100.0	0.0
77.5	100.0	0.0	7.3	100.0	0.0
66.9	100.0	0.0	6.3	100.0	0.0
57.7	100.0	0.0	5.4	100.0	5.0
49.8	100.0	0.0	4.7	94.9	80.3
42.9	100.0	0.0	4.1	14.6	14.6
37.1	100.0	0.0	3.5	0.0	0.0
32.0	100.0	0.0	3.0	0.0	0.0
27.6	100.0	0.0	2.6	0.0	0.0
23.8	100.0	0.0	2.2	0.0	0.0
20.5	100.0	0.0	1.9	0.0	0.0

Result source=testdata
Record No. = 14
Focal length = 100 mm.
Experiment type pia
Number distribution
Beam length = 51.0 mm.
Obscuration =0.9892
Volume Conc. = 0.0128 %
Log. Diff. =5.44
Model indp

D(v,0.5) = 4.3 µm
D(v,0.9) = 4.6 µm
D(v,0.1) = 4.0 µm
D(4,3) = 4.3 µm
D(3,2) = 4.3 µm
Span = 0.1
Spec. surf. area
1.40 sq.m./cc.

Figure 4.29 Number Distribution Motor Results Using Inner 28 Diode Rings, 20 May

Figure 4.30 SEM Photograph of Collected Combustion Products in Graphite Nozzle, 2.0% Al

Figure 4.31 SEM Photograph of Collected Combustion Products in Graphite Nozzle, 2.0% Al

Figure 4.32 SEM Photograph of Collected Combustion Products in Graphite Nozzle, 2.0% Al

Since the maximum scattering angle of the MALVERN was no longer limited by the rocket motor window, no rings of data were deleted from the analysis. As shown in Figures 4.33-4.36, the 22 and 26 May nozzle exhaust volume distribution D_{32} measurements made with the MALVERN were 127.1 and 97.6 microns respectively. The number distribution D_{32} measurements were 122.6 and 1.1 microns respectively. The 26 May results indicated a tri-modal volume distribution of particles. The number distribution was monomodal and dominated by particles of less than 2.6 micron diameters.

The 22 and 26 May internal motor environment D_{32}'s measured by the NPS system (Figures 4.37 and 4.38) were 4.4 and 4.6 microns. Although the background was not subtracted, the curve fit left little doubt that these measurements were of a reasonable accuracy.

During these four tests the D_{32} values obtained for the motor environment from both the MALVERN and NPS systems were in excellent agreement (within 7%). The D_{32} values obtained in the exhaust using the NPS system were consistent, but the system was not capable of measuring the very large particles observed by the MALVERN. The large particles are believed to originate from the RTV used for inhibiting and bonding.

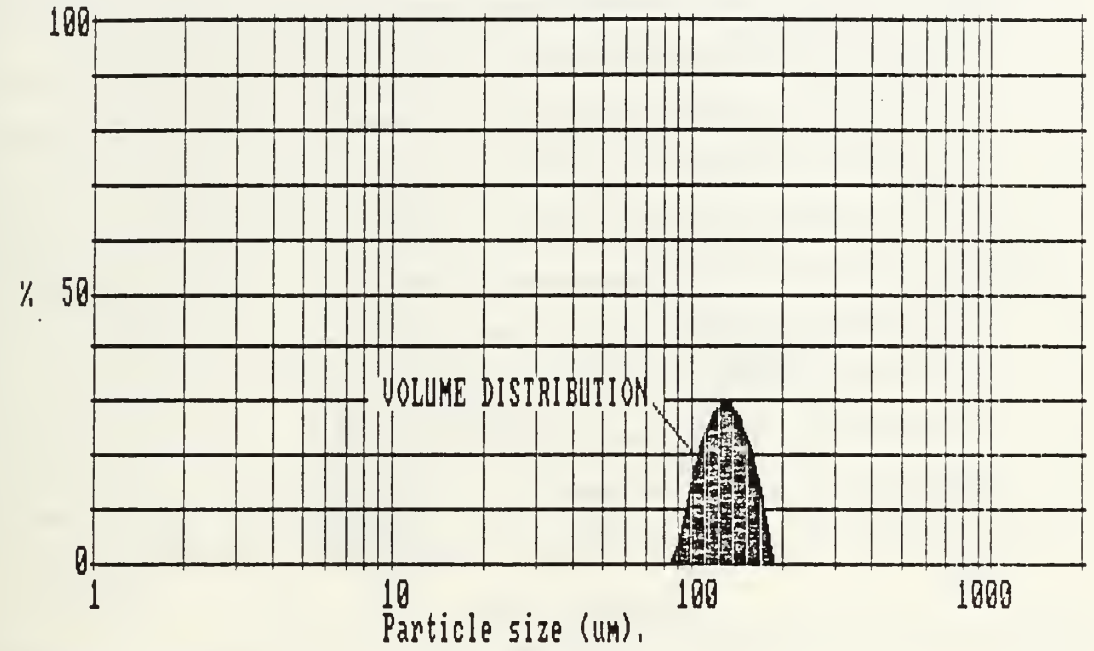

Size microns	under	% in band	Size microns	under	% in band	
188.0	100.0	10.1	17.7	0.0	0.0	Result source=testdata
162.0	89.9	23.7	15.3	0.0	0.0	Record No. = 15
140.0	66.2	28.6	13.2	0.0	0.0	Focal length = 100 mm.
121.0	37.6	25.6	11.4	0.0	0.0	Experiment type pia
104.0	12.0	11.8	9.8	0.0	0.0	Volume distribution
89.9	0.2	0.2	8.5	0.0	0.0	Beam length = 12.0 mm.
77.5	0.0	0.0	7.3	0.0	0.0	Obscuration =0.2248
66.9	0.0	0.0	6.3	0.0	0.0	Volume Conc. = 0.0973 %
57.7	0.0	0.0	5.4	0.0	0.0	Log. Diff. =5.57
49.8	0.0	0.0	4.7	0.0	0.0	Model indp
42.9	0.0	0.0	4.1	0.0	0.0	
37.1	0.0	0.0	3.5	0.0	0.0	D(v,0.5) = 128.9 µm
32.0	0.0	0.0	3.0	0.0	0.0	D(v,0.9) = 162.2 µm
27.6	0.0	0.0	2.6	0.0	0.0	D(v,0.1) = 102.4 µm
23.8	0.0	0.0	2.2	0.0	0.0	D(4,3) = 130.8 µm
20.5	0.0	0.0	1.9	0.0	0.0	D(3,2) = 127.1 µm
						Span = 0.5
						Spec. surf. area
						0.05 sq.m./cc.

Figure 4.33 Volume Distribution Exhaust Results, 22 May

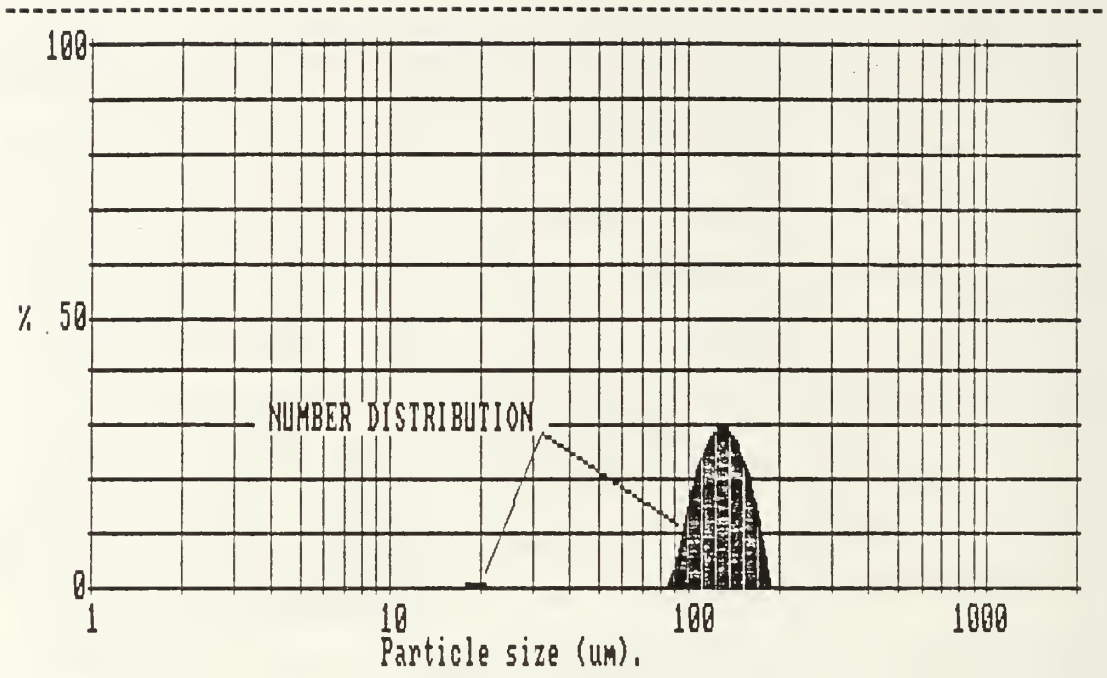

Size microns	under	% in band	Size microns	under	% in band
188.0	100.0	10.1	17.7	0.1	0.1
162.0	89.9	23.6	15.3	0.0	0.0
140.0	66.3	28.5	13.2	0.0	0.0
121.0	37.9	25.5	11.4	0.0	0.0
104.0	12.4	11.8	9.8	0.0	0.0
89.9	0.6	0.2	8.5	0.0	0.0
77.5	0.5	0.0	7.3	0.0	0.0
66.9	0.5	0.0	6.3	0.0	0.0
57.7	0.5	0.0	5.4	0.0	0.0
49.8	0.5	0.0	4.7	0.0	0.0
42.9	0.5	0.0	4.1	0.0	0.0
37.1	0.5	0.0	3.5	0.0	0.0
32.0	0.5	0.0	3.0	0.0	0.0
27.6	0.5	0.0	2.6	0.0	0.0
23.8	0.5	0.1	2.2	0.0	0.0
20.5	0.4	0.3	1.9	0.0	0.0

Result source=testdata
Record No. = 15
Focal length = 100 mm.
Experiment type pia
Number distribution
Beam length = 12.0 mm.
Obscuration =0.2248
Volume Conc. = 0.0973 %
Log. Diff. =5.57
Model indp

D(v,0.5) = 128.7 µm
D(v,0.9) = 162.1 µm
D(v,0.1) = 102.1 µm
D(4,3) = 129.6 µm
D(3,2) = 122.6 µm
Span = 0.5
Spec. surf. area
0.05 sq.m./cc.

Figure 4.34 Number Distribution Exhaust Results, 22 May

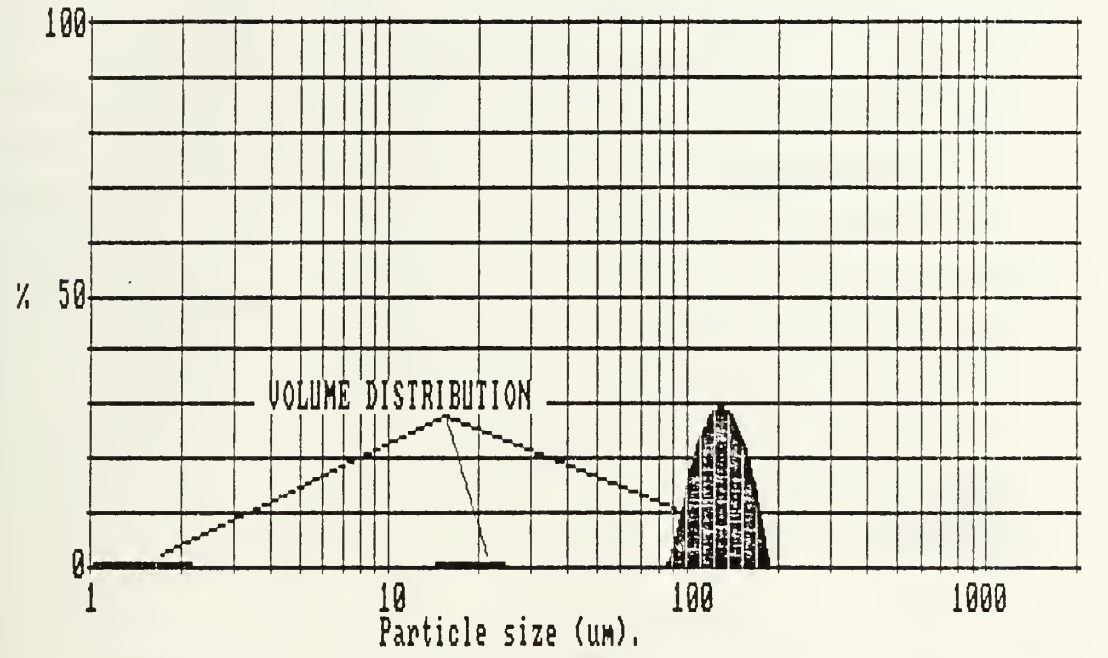

Size microns	under	% in band	Size microns	under	% in band
188.0	100.0	10.0	17.7	0.9	0.1
162.0	90.0	23.3	15.3	0.8	0.0
140.0	66.7	28.2	13.2	0.8	0.0
121.0	38.5	25.2	11.4	0.8	0.0
104.0	13.3	11.7	9.8	0.8	0.0
89.9	1.6	0.2	8.5	0.8	0.0
77.5	1.5	0.0	7.3	0.8	0.0
66.9	1.5	0.0	6.3	0.8	0.0
57.7	1.5	0.0	5.4	0.8	0.0
49.8	1.5	0.0	4.7	0.8	0.0
42.9	1.5	0.0	4.1	0.8	0.0
37.1	1.5	0.0	3.5	0.8	0.0
32.0	1.5	0.0	3.0	0.8	0.0
27.6	1.5	0.0	2.6	0.8	0.0
23.8	1.5	0.1	2.2	0.8	0.1
20.5	1.4	0.4	1.9	0.7	0.1

Result source=testdata
Record No. = 16
Focal length = 100 mm.
Experiment type pia
Volume distribution
Beam length = 12.0 mm.
Obscuration =0.1506
Volume Conc. = 0.0324 %
Log. Diff. =5.55
Model indp

D(v,0.5) = 128.4 µm
D(v,0.9) = 162.0 µm
D(v,0.1) = 101.3 µm
D(4,3) = 128.5 µm
D(3,2) = 97.6 µm
Span = 0.5
Spec. surf. area
0.05 sq.m./cc.

Figure 4.35 Volume Distribution Exhaust Results, 26 May

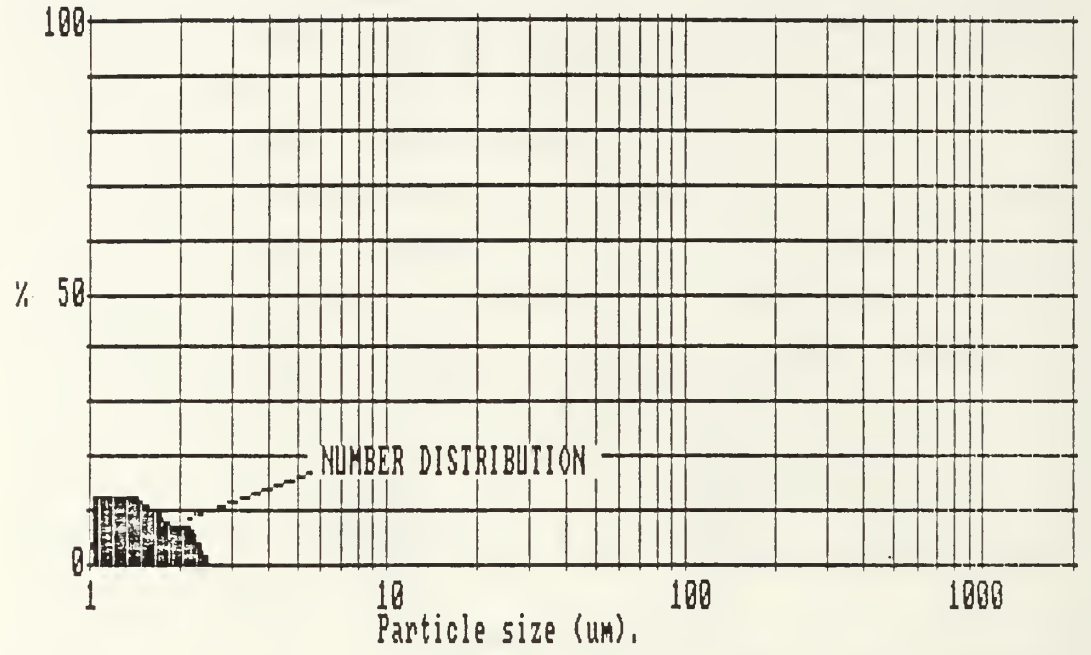

Size microns	under	% in band	Size microns	under	% in band
188.0	100.0	0.0	17.7	99.9	0.0
162.0	100.0	0.0	15.3	99.9	0.0
140.0	100.0	0.0	13.2	99.9	0.0
121.0	100.0	0.0	11.4	99.9	0.0
104.0	100.0	0.0	9.8	99.9	0.0
89.9	100.0	0.0	8.5	99.9	0.0
77.5	100.0	0.0	7.3	99.9	0.0
66.9	100.0	0.0	6.3	99.9	0.0
57.7	100.0	0.0	5.4	99.9	0.0
49.8	100.0	0.0	4.7	99.9	0.0
42.9	100.0	0.0	4.1	99.9	0.0
37.1	100.0	0.0	3.5	99.9	0.0
32.0	100.0	0.0	3.0	99.9	0.0
27.6	100.0	0.0	2.6	99.9	2.4
23.8	100.0	0.0	2.2	97.5	6.9
20.5	100.0	0.0	1.9	90.6	9.7

Result source=testdata
Record No. = 16
Focal length = 100 mm.
Experiment type pia
Number distribution
Beam length = 12.0 mm.
Obscuration =0.1506
Volume Conc. = 0.0324 %
Log. Diff. =5.55
Model indp

D(v,0.5) = 1.1 µm
D(v,0.9) = 1.9 µm
D(v,0.1) = 0.7 µm
D(4,3) = 1.3 µm
D(3,2) = 1.1 µm
Span = 1.1
Spec. surf. area
0.05 sq.m./cc.

Figure 4.36 Number Distribution Exhaust Results, 26 May

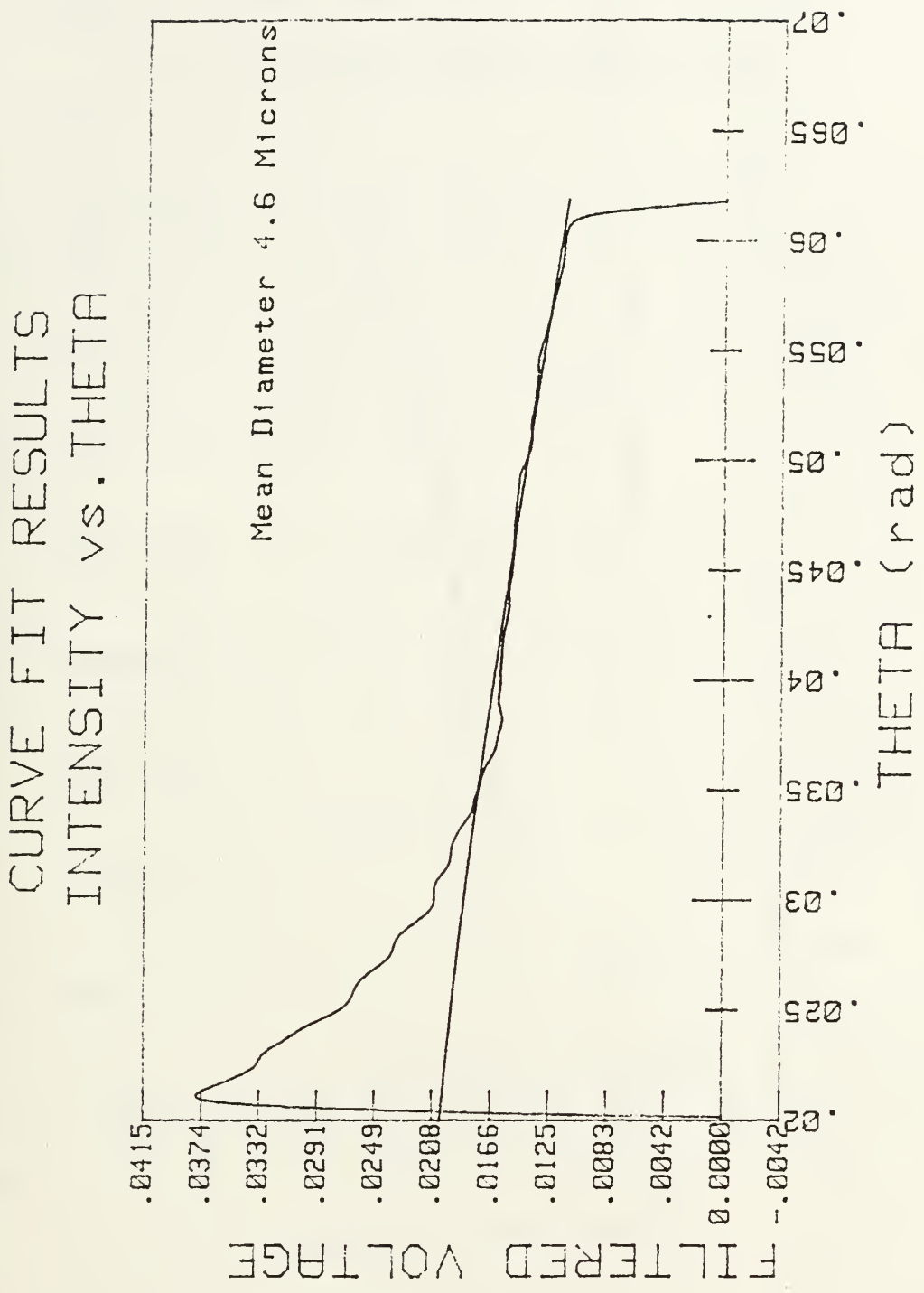

Figure 4.37 Motor Profile, 22 May

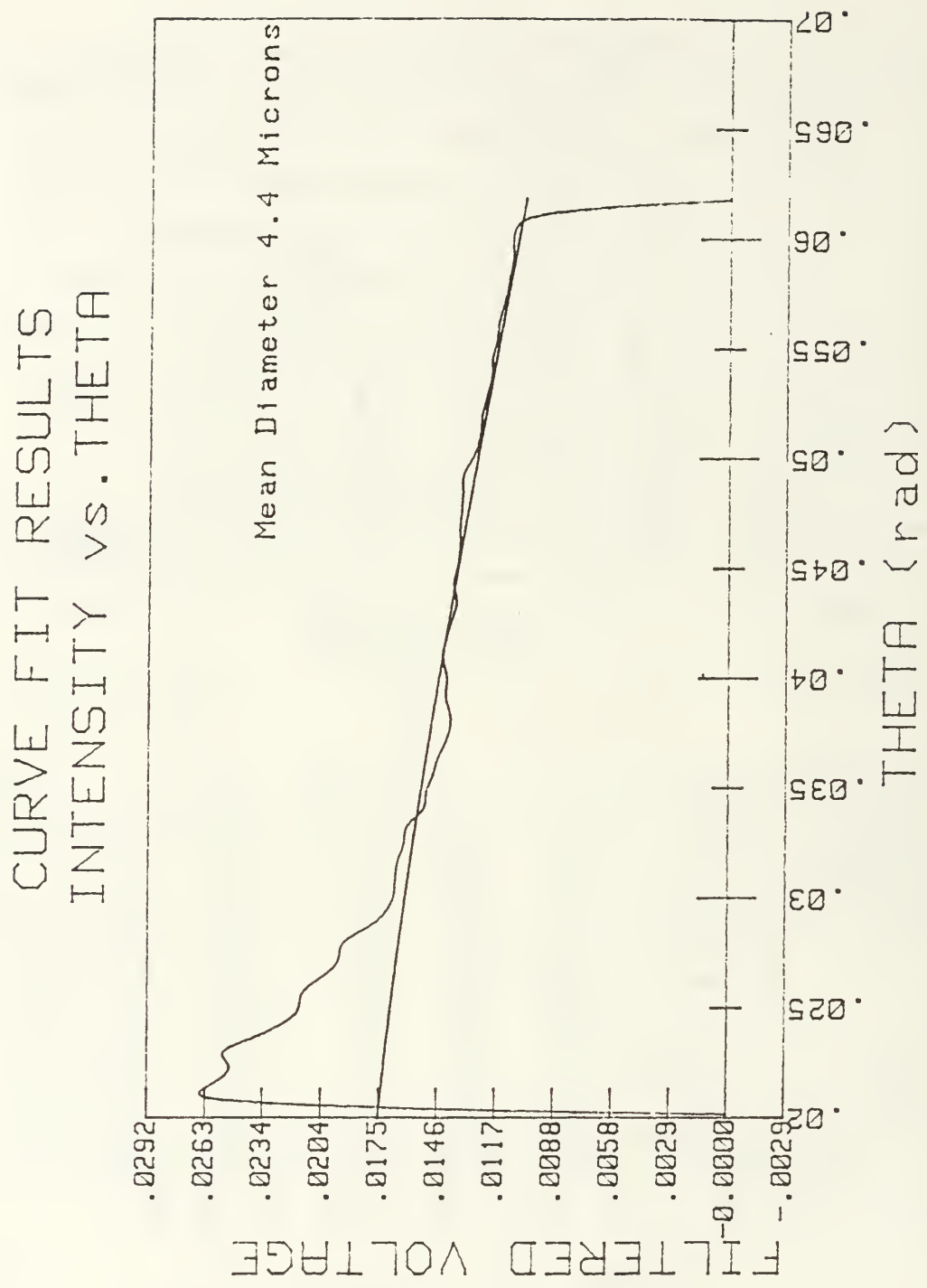

Figure 4.38 Motor Profile, 26 May

V. CONCLUSIONS AND RECOMMENDATIONS

The results of this investigation have shown that the measurement of particle size distribution and D_{32} can be made through both the exhaust jet and the motor. However, certain limitations and restrictions do exist, and must be resolved prior to determining if accurate measurements are possible.

Manufacture of the two-dimensional (2D) motor with the 50 mm windows should correct the large angle scattering problem that exist with MALVERN measurements across the motor windows. The 2D motor with its narrow internal port will reduce the level of obscuration, which should improve the accuracy of the MALVERN, but may lead to difficulties with achieving an adequate signal for the NPS system. Since the NPS and MALVERN light scattering systems provided repeatable and cross correlatable particle size data as evidenced by the test conducted on 19-26 May, the MALVERN has been verified to be as accurate as the NPS system for measuring the motor internal environment.

Contamination by large particles was evident throughout the testing phase. The most logical source of these large particles was the RTV material. The present propellant cutter is approximately 0.1 inches smaller in diameter than

the three-dimensional motor cavity. By reducing the difference in diameters of the motor cavity and the cutter, the quantity of RTV used for bonding could be reduced. Also, by ensuring the amount of excess RTV at the back of a center punched hole is minimized, exposure of large amounts of the bonding material to the hot combustion gases during the measurement period could be minimized. Testing might also be conducted to find an alternate and more acceptable bonding material, since it will also be required by the 2D motor.

Beam wander did not occur during this investigation. If it is evidenced by later investigators two possible cures are to change the spatial filter and collimator to produce a light beam with a larger diameter and to ensure that measurements are taken on the flat pressure plateaus.

A final recommendation is that a new linear diode array be purchased to replace the existing array. Until such time as this is feasible, the modification of the RDC1 program to delete the subtraction of background from the sample data should continue to be considered as an acceptable alternative to aid in accurate interpolation of the analysis data provided by the NPS system.

LIST OF REFERENCES

1. Harris, K.G., et. al., MEASUREMENTS OF PARTICULATES IN SOLID PROPELLANT ROCKET MOTORS, Naval Postgraduate School, Air Force Astronautics Laboratory Report, AFAL-TR-87-029, June 1987.

2. R.W. Hermsen, Aluminum Oxide Particle Size for Solid Rocket Motor Performance Prediction, AIAA 19th Aerospace Sciences Meeting, Jan 12-15, 1981.

3. Van de Hulst, H. C., Light Scattering by Small Particles, John Wiley and Sons, Inc., New York, 1957.

4. Dobbins, R. A., Crocco, L. and Glassman, I., Measurement of Mean Particle Sizes of Spray from Diffractively Scattered Light, AIAA Journal, v. 1, No. 8, pp. 1882-1886, 1963.

5. Mugele, R. A. and Evans, H. D., Droplet Size Distribution in Sprays, Industrial and Engineering Chemistry, Volume 43, pp. 1317-1324, 1951.

6. Abubakar, K., Particle Sizing in a Solid Rocket Motor Using the Measurement of Scattered Light, M. S. Thesis, Naval Postgraduate School, Monterey, California, March 1985.

7. Rosa, J. S., Particle Sizing in a Solid-Propellant Rocket Motor Using Scattered Light Measurements, M. S. Thesis, Naval Postgraduate School, Monterey, California, December 1985.

8. Horton, K. G., Particulate Sizing in a Solid-Propellant Rocket Motor Using Light Scattering Techniques, M. S. Thesis, Naval Postgraduate School, Monterey, California, June 1986.

9. Keith, M. G., Particle Sizing in a Solid Propellant Rocket Motor Using a Light Scattering Technique, M. S. Thesis, Naval Postgraduate School, Monterey, California, December 1986.

10. MALVERN INSTRUMENTS PARTICLE SIZER REFERENCE MANUAL, Spring Lane, MALVERN, Worcestershire, WR141AQ, England, Manual Version 3.0, 22 July 1986.

11. 2600 PARTICLE SIZER USER MANUAL, Spring Lane, MALVERN, Worcestershire, WR141AQ, England, Manual Version 2.1, 30 September 1985.

12. Harris, R. K., An apparatus for Sizing Particulate Matter in Solid Rocket Motors, M. S. Thesis, Naval Postgraduate School, Monterey, California, 1983.

INITIAL DISTRIBUTION LIST

		No. Copies
1.	Defense Technical Information Center Cameron Station Alexandria, Virginia 22304-6145	2
2.	Library, Code 0142 Naval Postgraduate School Monterey, California 93943-5002	2
3.	Department Chairman, Code 67 Department of Aeronautics Naval Postgraduate School Monterey, California 93943-5000	1
4.	Professor D. W. Netzer, Code 67 Nt Department of Aeronautics Naval Postgraduate School Monterey, California 93943-5000	1
5.	LCDR T. E. Pruitt, USN Naval Plant Representative Office (Strategic Systems Program Office) Lockheed Missiles & Space Co., Inc. P.O. Box 3504 Sunnyvale, California 94088-3504	2

DUDLEY KNOX LIBRARY
NAVAL POSTGRADUATE SCHOOL
MONTEREY CALIFORNIA 93943-5002

Thesis
P94675 Pruitt
c.1 Measurement of particle size distribution in a solid propellant rocket motor using light scattering.

Thesis
P94675 Pruitt
c.1 Measurement of particle size distribution in a solid propellant rocket motor using light scattering.

Measurement of particle size distributio
3 2768 000 73493 3
DUDLEY KNOX LIBRARY